Self-archived version of the article published in Energy Conversion and Management:

B. Ortega-Delgado, F. Giacalone, P. Catrini, A. Cipollina, A. Piacentino, A. Tamburini, G. Micale, "Reverse electrodialysis heat engine with multi-effect distillation: Exergy analysis and perspectives" - Energy Conversion and Management 194 (2019) 140–159.
https://doi.org/10.1016/j.enconman.2019.04.056

Reverse electrodialysis heat engine with multi-effect distillation: exergy analysis and perspectives

B. Ortega-Delgado, F. Giacalone, P. Catrini, A. Cipollina*, A. Piacentino, A. Tamburini, G. Micale
Dipartimento di Ingegneria, Università degli Studi di Palermo (UNIPA)
Viale delle Scienze Ed.6, 90128, Palermo (Italy)
e-mail: andrea.cipollina@unipa.it

ABSTRACT

The increasing worldwide energy demand is rising the interest on alternative power production technologies based on renewable and emission-free energy sources. In this regard, the closed-loop reverse electrodialysis heat engine is a promising technology with the potential to convert low-grade heat into electric power. The reverse electrodialysis technology has been under investigation in the last years to explore the real potentials for energy generation from natural and artificial solutions, and recent works have been addressing also the potential of its coupling with regeneration strategies, looking at medium and large energy supply purposes. In this work, for the first time, a comprehensive exergy analysis at component level is applied to a reverse electrodialysis heat engine with multi-effect distillation in order to determine the real capability of the waste heat to power conversion, identifying and quantifying the sources of exergy destruction. In particular, sensitivity analyses have been performed to assess the influence of the main operating conditions (i.e. solutions concentration and velocity) and design features (aspect ratio of the pile), characterizing the most advantageous scenarios and including the effect of new generations of membranes. Results show that the multi-effect distillation unit is the main source of exergy destruction. Also, using high-performing membranes, inlet solutions concentration and velocity of 4.5 – 0.01 mol/L and 0.2 – 0.36 cm/s, respectively, a global exergy

efficiency of 24% is reached for the system, proving the high potential of this technology to sustainably convert waste heat into power.

Keywords

salinity gradient power; SGP; NaCl; osmotic power; chemical exergy; energy conversion

1. INTRODUCTION

The actual scenario of energy crisis and concern about global warming is leading to seek new power production technologies as alternatives to classic methods based on fossil fuels, which significantly contribute to the increase of the average global temperature of the planet. Moreover, large amounts of heat from different industrial processes are rejected to the atmosphere without further use, in some cases up to 70% of the input energy [1]. This valuable heat (called waste heat), at temperatures below 100 °C, may be used to generate electricity by means of a suitable heat-to-power conversion technology. In this regard, there are several techniques available working at temperatures above 100 °C, such as the steam Rankine cycle, the organic Rankine cycle, the Kalina cycle, the thermoelectric generator or the free piston Stirling engine, while there is a lack of technologies able to recover waste heat below that temperature level.

One of the unexploited and emission-free energy sources that has gained interest during the last years is the salinity gradient energy (SGE). This energy source comes from the difference of chemical potential between two salt solutions with different concentrations. In nature this kind of energy can be drawn from the natural mixing of rivers and lakes into the sea. One of the biggest advantages of this energy source relies on its huge theoretical potential, about 2.7 TW of power according to [2], however, it has not been exploited on large scale so far.

There are mainly two different membrane-based technologies able to harvest the energy from SGE sources, namely pressure-retarded osmosis and reverse electrodialysis (RED). A comparison and evaluation of the two methods is reported in [3]. In the first case, semi-permeable membranes are used between a draw (high concentrated solution) and a feed (low concentrated solution) streams. If the draw solution is pressurized below the osmotic pressure difference of both streams, a water flux is induced from the feed to the draw. This pressurized volume of water can be later discharged to a turbine to generate electricity. In the second case, the RED technique generates directly electric energy by the controlled mixing of two solutions with different salinities using ion exchange membranes (IEM). This concept was first introduced at the end of the nineteenth century [4].

Focusing on the RED process, in 1954 Pattle [5] reported that continuous electric power could be produced by harnessing the energy released from the mixing of river water and seawater by means of an 'hydroelectric pile', composed of alternative channels of water and salt water, separated by IEMs. However, the first experiments performed provided low values of electric power generation. Since then, a number of relevant studies on the RED process have been conducted, mainly aimed at increasing the performance by the enhancement of the membrane's features. For instance, Weinstein et al. [6] presented one of the first mathematical models for RED systems. Jagur-Grodzinski and Kramer [7] analysed the RED process obtaining also an acid and a base as by-products, reaching a power density (power produced per square meter of membrane) of 1 W/m^2. More recently, Veerman et al. [8] studied the reduction of efficiency losses associated with the ionic shortcut currents in a RED stack. The efficiency losses decreased from 25 to 5% by optimizing the membranes and channels resistance. Vermaas et al. [9] evaluated experimentally the effect of the intermembrane distance on the RED performance. They obtained that reducing this distance could improve the efficiency, reaching a maximum power density of 2.2 W/m^2. Daniilidis et al. [10] reported power densities of about 6.7 W/m^2 in laboratory using 5 – 0.01 M artificial solutions (concentrate – dilute). Long et al. [11] analysed the effect of the channel thickness and solutions flow rate on the performance, determining that there are optimal values leading to a significant increase of the efficiency. Besides, the same authors [12] used a multi-objective optimization process to identify the operating variables values leading to a compromise between maximum power density and maximum power conversion efficiency in a RED system.

The first RED pilot plant using natural and artificial solutions was built in Trapani (Italy), within the framework of the REAPower project [13]. By using natural solutions from saltworks (brackish water – brine), a power output of 330 W and power density of 1.6 W/m^2 were achieved. Conversely, with artificial sodium chloride (NaCl) solution these values increased up to 700 W and 3.6 W/m^2, respectively. This RED pilot plant demonstrated for the first time the feasibility of the technology under real conditions.

However, a major drawback of the RED technology operated in open-loop configuration is the unavailability of natural high salinity water sources in areas of power demand. This may be solved by the use of a closed-loop RED-Heat Engine (RED-HE), where ad-hoc artificial saline solutions are adopted, thus allowing for the increase of the salinity gradient (driving force of the process) and significantly improving the performance of the RED unit. The use of artificial salt solutions permits to purposively select the ones with better thermo-physical properties for the process. In addition, issues related with the fouling of the membranes when using natural

water sources disappear. The concept was first patented in 1979 by Loeb [14], who introduced the RED-HE concept with the regeneration of the outlet RED concentrate and dilute solutions by a thermal separation process. The RED-HE does not have any environmental risk associated with the operation at high temperature using hazardous substances, and it is not constrained by the water resource location. Another important advantage of the closed-loop RED-HE is the relatively low temperature of the heat source (below 100 °C), which enlarges the applicability of the technology, compared with other power cycles.

The closed-loop RED-HE is being investigated within the framework of the EU project RED-Heat-to-Power [15]. In this project, two different schemes are assessed depending on the regeneration technique: solvent extraction, using for instance multi-effect distillation (MED) or membrane distillation (MD) processes, and solute extraction, using thermolytic salts, such as ammonium bicarbonate (NH_4HCO_3).

The multi-effect distillation technology, high energy-intensive, has been used in the food and chemical industry since the beginning of the twentieth century, and it has been widely applied for seawater desalination as well. There are a number of mathematical MED models reported in the literature. One of the first models was proposed by El-Sayed and Silver [16], based on simplifying assumptions, such as constant properties of solutions during the process. El-Dessouky et al. [17] presented a detailed MED steady-state model, based on mass and energy balances, including the dependence of the water thermo-physical properties on the temperature and concentration. Also, they considered the non-condensable gases effect on heat transfer, the thermodynamic losses of the vapour across the effects, and assumed constant heat transfer areas both for evaporators and preheaters. Results obtained showed that the performance of the MED is almost independent of the top brine temperature, while it is greatly affected by the number of effects. Another interesting work was presented by Mistry et al. [18], who developed a detailed model for the MED process, providing more detailed results and relying on fewer assumptions. Recently, Ortega-Delgado et al. [19] presented an advanced forward-feed MED model able to simulate a wide range of design and operating conditions (high number of effects and feedwater salinity), particularly adequate for the analysis of the RED-MED integrated system.

The RED-HE scheme with solute extraction has been analysed in the literature by several authors. Luo et al. [20] proposed a thermal-driven electrochemical generator for waste heat conversion to electricity, using a distillation column and NH_4HCO_3 as working fluid. They proved the feasibility of this integration and obtained a power density of 0.33 W/m^2 and a RED exergy efficiency of 31%. Cusick et al. [21] presented a RED-HE using microbial cells and

NH_4HCO_3, with a continuous salinity regeneration of the solutions. They obtained a maximum power density of 3 W per square meter of projected cathode area (equivalent to ~0.3 W/m^2 of cell pair) using domestic wastewater, with an energy recovery of 30%. Kwon et al. [22] presented a parametric analysis of a NH_4HCO_3 RED system for the conversion of waste heat into electricity, obtaining a maximum power density of 0.77 W/m^2. Hatzell et al. [23] compared the power and hydrogen production in a closed-loop NH_4HCO_3 RED system, and reported that if hydrogen gas can be recovered, this system may produce 150% more electricity than the conventional RED unit. More recently, Bevacqua et al. [24] experimentally assessed the performance of a RED-HE using NH_4HCO_3, and they obtained a maximum power density of 2.42 W/m^2 of cell pair at the lower feed flow velocity investigated. They concluded that, although this technology can be comparable with the RED-HE with NaCl as working fluid, further improvement in the membranes features should be accomplished. Bevacqua et al. [25] presented a model for the previously described cycle, which was validated by experimental data. In addition, they performed a sensitivity analysis of the performance as a function of the inlet solutions concentration and velocity. The results obtained indicated that a power density of 9 W/m^2 and a global exergy efficiency of 22% could be reached at the best-performing operating conditions and using membranes with enhanced properties.

Regarding RED-HE with solvent extraction scheme, only few works can be found in the literature. In particular, Long et al. [26] analysed a RED unit coupled to a membrane distillation regeneration stage. They performed simulations by varying the heat source temperature and the NaCl feed concentration, and obtained a maximum thermal efficiency value of 1.15% for the highest concentration (5 mol/kg). Micari et al. [27] assessed the performance of a RED-MD HE, with varying operating conditions. They obtained maximum thermal and exergetic efficiencies of 2.8% and 16.5%, respectively, using IEMs and MD modules with improved properties. Tamburini et al. [28] presented a performance evaluation of the RED-HE system considering different salt solutions and regeneration methods. Specifically, the multi-effect distillation process was considered as regeneration stage using a simplified model and efficiency indicators obtained from literature data, such as the specific thermal energy consumption. Preliminary results showed that the closed-loop heat engine can reach thermal and exergetic efficiencies up to 15% and 85%, respectively, using membranes with enhanced properties. They also suggested the need to carry out further performance analyses with a comprehensive modelling of the RED and MED units in order to identify sources of exergy destruction and improve the overall efficiency of the technology. In this regard, Giacalone et al. [29] presented an extensive exergy analysis of the standalone RED unit, using a detailed

mathematical model of the process. They analysed the effect of the main operating variables (solutions concentration and velocity) and considered all sources of irreversibility within the RED process. Results highlighted the large dependence of the system's performance on the solutions concentration, obtaining that the water flux due to osmosis had the highest destructive effect on the RED exergy efficiency when high salinity gradient was used.

More recently, Hu et al. [30] presented an energetic analysis of the RED-MED HE integrated system. They found that the global energy efficiency of this system could reach about 1% with a HC solution concentration of 5.4 mol/kg and an external hot water temperature of 95°C, using 10 effects. Palenzuela et al. [31] carried out a performance analysis of a RED-MED HE dependent on the main operating parameters. They obtained a maximum overall thermal and exergy efficiencies of 1.4% and 6.7%, respectively, considering current state-of-the-art IEMs, and 6.6% and 31% when using membranes with enhanced properties. In this work, only the overall exergy results were presented, but no detailed exergy analysis was performed. They also suggested the need of further evaluation of the exergy losses in the RED-MED system. A theoretical study of the suitability of different working solutions for RED-HE with single multi-stage evaporative regeneration unit was carried out by Giacalone et al. [32], obtaining that acetate salts (KAc, CsAc) can perform better than conventional NaCl solutions due to their higher solubility and free Gibbs energy of mixing.

Despite the above-mentioned previous works, a detailed and comprehensive exergy analysis of the RED-HE has not been performed yet in the literature, which is needed to reveal the maximum theoretical energy conversion potential of the technology and identify and quantify the sources of irreversibility. Exergy analysis is an engineering tool commonly used in the design, assessment and optimization of thermal systems. There are a number of relevant works that have applied exergy analysis to evaluate diverse energy conversion processes in the last years. For instance, Bi et al. [33] presented an exergy analysis of a ground-source heat pump for building heating/cooling, leading to identify the compressor and ground heat exchanger as the main sources of exergy loss in the system. Karellas and Braimakis [36] evaluated the performance of a tri/co-generation system producing heat, power, and refrigeration, by means of an ORC cycle and a vapour compression cycle. They applied an exergy analysis under two different operation modes and reported that half of the total irreversibility took place in the condenser, followed by the turbine and heat exchangers. Ahmadi et al. [38] performed an exergy analysis and multi-objective optimization to a combined cycle power plant, identifying the combustion chamber as the main source of exergy destruction. Hepbasli [40] conducted a review on low-exergy heating and cooling systems for sustainable buildings design, where

exergy analysis is used to quantify the potential for enhancing the equivalence between the energy source and the energy demand in buildings. Also, exergy analysis has been used in works related to SGE systems for energy conversion, such as the study of Emdadi et al. [43]. They used it to calculate the maximum energy potential from a natural SGE system mixing seawater and river water. More examples can be found in Hepbasli [44], who presented an extensive review of exergetic analyses and assessment of different energy systems based on renewable energy sources.

A detailed exergy analysis on a RED-MED HE scheme at component level has been carried out in this work for the first time, analysing the effect of the main operating and design conditions on the global performance of the RED-MED HE. Mathematical models for each subsystem have been integrated in order to simulate the operation of the overall system. Firstly, a reference case has been selected to evaluate the main performance indicators (exergy and thermal efficiency, power density, specific thermal energy consumption) with usual design and operating conditions. Later, the effect of the main sources of irreversibility on the exergy efficiency has been analysed as a function of the electric current in the RED unit. Also, sensitivity analyses of the exergy efficiency, at global and component level, have been carried out depending on main operating and design parameters of the RED-HE: inlet solutions concentration, inlet velocity and aspect ratio of the membranes. Finally, a perspective analysis of the technology is presented by evaluating the overall exergy efficiency using high-performing membranes in the RED unit.

2. DESCRIPTION AND MODELLING OF THE SYSTEM

The entire model has been implemented in Engineering Equation Solver (EES) [45] software and it is constituted by four sections:

(i) Reverse electrodialysis process model, which is a mono-dimensional model describing all the main phenomena involved in the power generation process;

(ii) Multi-effect distillation process model, based on mass and energy balances applied on each component constituting the plant;

(iii) Model integration, where the RED model and the MED model are coupled including also two mixing processes of the solutions;

(iv) Exergy analysis, which provides the equations to evaluate the exergy flux and the exergy efficiency definition in each component of the system.

2.1 Reverse electrodialysis unit

The reverse electrodialysis technology is a membrane-based process that directly converts the electrochemical energy into electricity. The main element of this process is the ion-exchange membrane, which can be cationic (CEM) or anionic (AEM), stacked in series with alternative positions (see Fig. 1). The RED unit is constituted by repetitive units called cell pair. A cell pair consists of two membranes, an AEM and CEM, and two channels, one for the dilute or low concentration solution (LC) and one for the high concentration solution (HC). The dilute ($\dot{m}_{LC,in}$) and concentrate ($\dot{m}_{HC,in}$) solutions are pumped into the corresponding channels formed between the membranes, which are supported by spacers (or with profiled membranes). Cations and anions pass naturally through the membranes generating a differential of electrochemical potential between them. At both extremes of the unit, two electrodes are used, together with an external resistance, to close the circuit and generate the electricity by means of a reversible redox reaction (rinse solution).

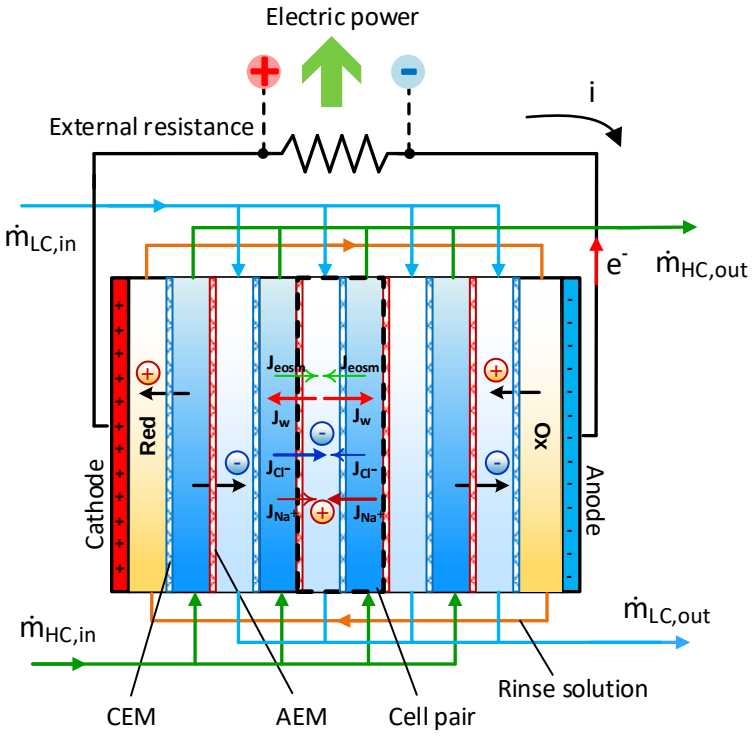

Fig. 1. Scheme of the reverse electrodialysis unit.

The RED unit has been modelled using the method described by Giacalone et al. [29]. The mathematical model is mainly based on mass and transport balances along the longitude of the system, together with the equations associated with the equivalent electric circuit, following a hierarchical structure. The model has been validated against experimental data in [29]. The model includes some simplifying assumptions, such as considering a mono-dimensional system

where the concentrations, fluxes, currents, etc. vary only along the channel length (L), which is discretized in N_k=40 elements. Also, the parasitic currents have been neglected. Conversely, the effects of concentration polarization phenomena in the membranes and pressure drop along the channels have been considered.

The low hierarchical level of the model contains all the equations associated with the cell pair, solved within the discretized domain over the length of the membranes. The electro-motive force E_{cell} (V) produced in each cell pair is determined with Eq. (1):

$$E_{cell}(k) = E_{CEM}(k) + E_{AEM}(k) \cong 2\alpha_{av}(k)\frac{RT}{F}\ln\left(\theta_{IEM}^{HC}(k)\cdot\theta_{IEM}^{LC}(k)\frac{m_{HC}(k)\cdot\gamma_{HC}(k)}{m_{LC}(k)\cdot\gamma_{LC}(k)}\right) \quad (1)$$

where α_{av} (-) is the average permselectivity of the membranes, which represents their selectivity to the passage of counter ions (cations or anions) and rejection of co-ions, R (J/mol·K)) is the gas constant, T (K) is the average temperature of the solutions, F (A·s/mol) is the Faraday constant, θ (-) is the polarization coefficient of the solution (either concentrated or diluted), which accounts for the different solutions concentration in the membrane interphase with respect to the bulk due to the reduction of the mass transfer coefficient near the membrane [46], m (mol/kg) is the molality of the solution, and γ (-) is the activity coefficient of the solution, calculated with Eq. (A.1) of Appendix A.

The electrical resistance R_{cell} (Ω) of the cell pair is the sum of the areal resistances of the channels, R_{HC} and R_{LC}, and the IEMs, R_{CEM} and R_{AEM}:

$$R_{cell}(k) = [R_{HC}(k) + R_{LC}(k) + R_{CEM}(k) + R_{AEM}(k)]\cdot\frac{1}{b\Delta x} \quad (2)$$

where b (m) is the width of the membrane, and Δx (m) is the length of the discretized element.

The electrical resistance of the channels R_{sol} (Ω·m^2) are determined by Eq. (3):

$$R_{sol}(k) = s_f\cdot\frac{\delta_{sol}}{\Lambda_{sol}(k)\cdot C_{sol}(k)} \quad (3)$$

where s_f (-) is the spacer shadow factor, a parameter accounting for the increase of the resistance caused by the presence of the spacer, with a value of 1.5625 [29], δ_{sol} (m) is the channel width of the solution, Λ_{sol} (S·m^2/mol) is the equivalent conductivity of the solution, calculated as shown in Appendix A, and C_{sol} (mol/L) is the molar concentration of the solution (either concentrated, HC, or diluted, LC).

The electric current i (A) generated in each branch of the equivalent electric circuit is determined by Eq. (4):

$$N_{cp} \cdot E_{cell}(k) = N_{cp} \cdot R_{cell}(k) \cdot i(k) + R_{blank} I / A_{cp} + E_{stack} \quad (4)$$

where N_{cp} (-) is the number of cell pairs, R_{blank} ($\Omega \cdot m^2$) is the electrical resistance of the electrodic compartments, A_{cp} (m^2) is the membrane area of a cell pair, E_{stack} (V) is the voltage drop in the external resistance R_L (Ω), calculated with Eq. (5):

$$E_{stack} = R_L \cdot I \quad (5)$$

where I (A) is the current passing through the external resistance, evaluated as:

$$I = \sum_{k=1}^{N_k} i(k) \quad (6)$$

In the high hierarchical level of the model, related to the stack, the gross power P_{gross} (W) produced is obtained with Eq. (7):

$$P_{gross} = E_{stack} \cdot I \quad (7)$$

The pumping power consumed in the RED unit $P_{pump,RED}$ (W) is calculated as a function of the pressure drop of the solutions flowing along the channels (see Appendix B), determined by Eq. (8):

$$P_{pump,RED} = \frac{\Delta p_H Q_{HC}}{\eta_{p,HC}} + \frac{\Delta p_L Q_{LC}}{\eta_{p,LC}} \quad (8)$$

where Q (m^3/s) is the volumetric flow rate of the solution, and η_p (-) the isentropic efficiency of the pumps.

The gross power density $P_{d,gross}$ (W) (per square meter of cell pair) is determined with Eq. (9):

$$P_{d,gross} = \frac{P_{gross}}{A_{cp} N_{cp}} \quad (9)$$

and the net power density $P_{d,net}$ (W) is calculated by Eq. (10):

$$P_{d,net} = P_{d,gross} - P_{pump,RED} \quad (10)$$

There are ohmic losses P_{loss} (W) associated with the internal resistance of the stack, evaluated with Eq. (11):

$$P_{loss} = \sum\nolimits_k R_{cell}(k) \cdot i^2(k) + R_{blank} \cdot I^2 \quad (11)$$

The transport equations determine the water and salt fluxes through the IEMs. In particular, the salt flux J_s (mol/($m^2 \cdot s$)) is the sum of a coulombic term J_{coul}, caused by the migration of the

counter ions, and a diffusive term J_{diff}, generated by the co-ions diffusion, as shown in Eq. (12):

$$J_s(k) = J_{coul}(k) + J_{diff}(k) = \frac{i(k)}{b\Delta x \cdot F} + \frac{2P_s}{\delta_m}[C_{HC}(k) - C_{LC}(k)] \quad (12)$$

where P_s (m^2/s) is the salt permeability, δ_m (m) is the membrane thickness (assumed to be equal for both IEMs), and C_{HC} (mol/L) and C_{LC} (mol/L) are the molar concentration of the HC solution and LC solution, respectively. The diffusive term reduces the salinity gradient and therefore the driving force of the process.

The water flux J_w (mol/(m^2·s)) is also formed by the sum of two terms: the osmostic flux J_{osm}, caused by the difference of osmotic pressure between the two solutions, directed from the dilute to the concentrate solution (reducing the driving force), and the electro-osmotic flux J_{eosm}, produced by the water pass in the solvation shell formed around the salt ions, from the concentrate to the dilute solution (thus increasing the driving force):

$$\begin{aligned} J_w(k) &= J_{osm}(k) + J_{eosm}(k) \\ &= -2\nu RTP_w[C_{HC}(k)\phi_{HC}(k) - C_{LC}(k)\phi_{LC}(k)] \cdot \frac{\rho_w}{M_w} + n_H J_s(k) \end{aligned} \quad (13)$$

where ν is the number of ions, P_w (m/(Pa·s)) is the water permeability, ϕ (-) is the osmotic coefficient of the solution, calculated with Eq. (A.2), ρ_w (kg/m^3) is the density of water, M_w (g/mol) is the molar mass of water, and n_H (-) is the hydration number of the salt (assumed to have a value of 7 according to [47]).

The thermodynamic properties of the solutions (density, conductivity, diffusivity and viscosity) are discussed in Section 2.3, and the membrane properties (permselectivity, electrical resistance, water permeability and salt permeability) are reported in Appendix A.

The salt and global mass balances are also applied in each element k of the discretized membrane domain, considering a counter-current flow, both for the concentrate solution HC (Eqs. (14) and (15)):

$$C_{HC}(k+1) \cdot Q_{HC}(k+1) = C_{HC}(k) \cdot Q_{HC}(k) - J_s(k) \cdot b\Delta x \quad (14)$$

$$\rho_{HC}(k+1) \cdot Q_{HC}(k+1) = \rho_{HC}(k) \cdot Q_{HC}(k) - J_w(k) \cdot b\Delta x \rho_w / M_w - J_s(k) \cdot b\Delta x M_s \quad (15)$$

where $C_{HC}(k+1) \cdot Q_{HC}(k+1)$ and $\rho_{HC}(k+1) \cdot Q_{HC}(k+1)$ are the salt molar flow rate (mol/s) and total mass flow rate (kg/s) exiting from the element k, respectively; $C_{HC}(k) \cdot Q_{HC}(k)$ and $\rho_{HC}(k) \cdot Q_{HC}(k)$ are the salt molar flow rate (mol/s) and total mass flow rate (kg/s)

entering the element k, respectively; M_s (g/mol) is the molar mass of the salt. In these equations, C is in mol/m^3.

Similarly, the salt and global mass balances for the dilute solution LC are determined by Eqs. (16) and (17):

$$C_{LC}(k) \cdot Q_{LC}(k) = C_{LC}(k+1) \cdot Q_{LC}(k+1) + J_s(k) \cdot b\Delta x \tag{16}$$

$$\rho_{LC}(k) \cdot Q_{LC}(k) = \rho_{LC}(k+1) \cdot Q_{LC}(k+1) + J_w(k) \cdot b\Delta x\rho_w + J_s(k) \cdot b\Delta x M_s \tag{17}$$

2.2 Multi-effect distillation unit

The multi-effect distillation process is a thermally driven separation process, generally applied in the seawater desalination field. In the MED process, the salt solution is vaporized in falling-film heat exchangers placed inside pressure-decreasing vessels, called effects. A forward-feed MED arrangement has been selected, which is depicted in Fig. 2. This configuration is preferred when dealing with high salinity feedwater and high heating steam temperatures, due to the thermal losses caused by the boiling point elevation (BPE) that are lower (the maximum concentration is reached in the effect of lower temperature). Each effect is basically composed of a falling-film heat exchanger, a demister to remove the droplets from the vapour, and a preheater of the feedwater. The only external energy introduced in the process takes place in the evaporator of the first effect, generally with saturated steam at a certain temperature. In this case, waste heat coming from any industrial process is used as the input energy to the MED plant. The feedwater is sprayed over the tubes of the evaporator where part of the solvent is evaporated increasing the concentration of the remaining solution collected on the bottom of the effect. Part of the generated vapour is used to preheat the feedwater, while the rest is directed to the second evaporator, where the same process is repeated, at lower pressure and temperature. Starting from the second effect, the incoming brine flashes generating additional flash vapour. The condensate is collected in the flashing boxes, where extra vapour is produced as well. The vapour generated in the last effect condenses in the end condenser, which is cooled by an external source, such as river water. Finally, the concentrated solution is extracted from the last effect and the distillate stream from the last flashing box.

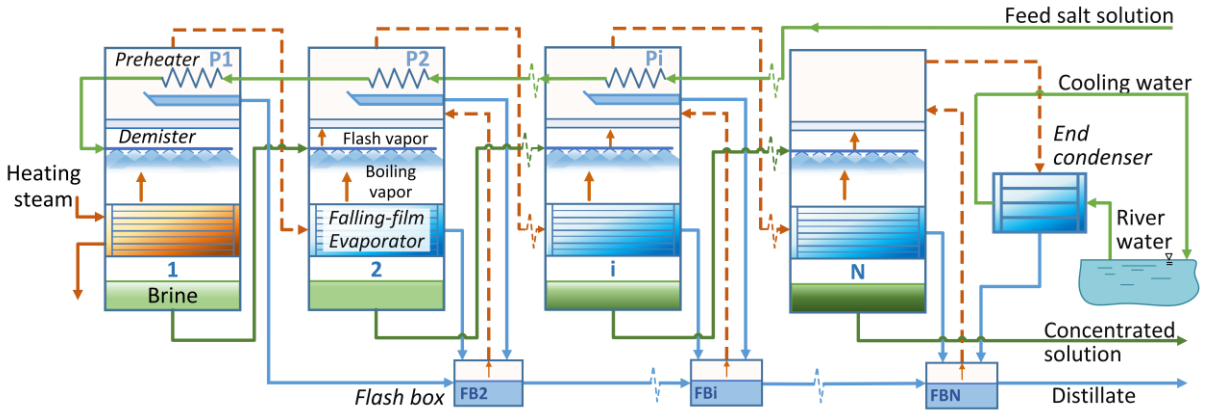

Fig. 2. Scheme of the forward-feed multi-effect distillation unit.

The mathematical MED model from Ortega-Delgado et al. [19] has been adopted because it is very flexible, detailed and permits the simulation of a high number of effects (>30) using high salinity feedwater. The model, validated in [19], is based mainly on mass and energy balances applied on each component of the plant, along with the heat transfer equations for the heat exchangers (evaporators, preheaters and end condenser). Given a low number of inputs (which can be easily exchanged with the outputs), the model determines the main thermodynamic (temperature, pressure, concentration, flow rate, enthalpy, etc.) and design variables (heat exchanger areas, number of evaporator tubes, vapour velocities, pressure losses, etc.). The model relies on several simplifying assumptions, such as neglecting the thermal losses to the environment and the presence of non-condensable gases, assuming saturation conditions at the inlet and outlet of the evaporators, salt-free distillate, and also uses temperature-based correlations for the determination of the overall heat transfer coefficients of the heat exchangers [48]. For the sake of brevity, only some representative equations of the model are shown. More details are provided in [19]. The pumping power requirement in the MED unit, $P_{pump,MED}$ (W), has been obtained as the sum of the pumping needed to overcome the pressure due to height of the unit ($\Delta p_{MED,H}$), the increase of pressure of the outlet concentrate ($\Delta p_{MED,HC,out}$) and distillate ($\Delta p_{MED,dist,out}$) solutions, and the pressure losses in the end condenser ($\Delta p_{MED,cooling}$), determined by Eq. (18):

$$P_{pump,MED} = \frac{\Delta p_{MED,H} \cdot Q_{MED,HC,in}}{\eta_{p,F}} + \frac{\Delta p_{MED,HC,out} \cdot Q_{MED,HC,out}}{\eta_{p,HC}} + \frac{\Delta p_{MED,dist,out} \cdot Q_{MED,dist,out}}{\eta_{p,dist}} + \frac{\Delta p_{MED,cooling} \cdot Q_{cw}}{\eta_{p,cw}} \quad (18)$$

where $Q_{MED,HC,in}$ and $Q_{MED,HC,out}$ (m^3/s) are the volumetric flow rates of the HC solution entering and exiting the MED unit, respectively, $Q_{MED,dist,out}$ (m^3/s) is the volumetric flow rate

of the distillate produced, Q_{cw} (m^3/s) is the volumetric flow rate of the cooling water, and $\eta_{p,F}$, $\eta_{p,HC}$, $\eta_{p,dist}$, and $\eta_{p,cw}$ are the isentropic efficiencies of the feed pump, HC pump, distillate pump and cooling water pump, respectively. The pressure drops Δp (Pa) are calculated as reported in Appendix B.

The global mass balance and salt balance are determined in Eq. (19) and Eq. (20), respectively:

$$\dot{m}_F = \dot{m}_B + \dot{m}_D \tag{19}$$

$$\dot{m}_F X_F = \dot{m}_B X_B \tag{20}$$

where $\dot{m}_F$ (kg/s) is the total mass flow rate of feedwater, $\dot{m}_B$ (kg/s) the total mass flow rate of brine (concentrated solution), $\dot{m}_D$ (kg/s) the total mass flow rate of distillate, X_F (ppm) is the salinity of the feedwater, and X_B (ppm) is the salinity of the brine.

The total distillate water flow rate produced in the MED unit $\dot{m}_D$ (kg/s) is calculated as the sum of the distillate water flow rate produced in each effect by evaporation, $\dot{m}_{Di}$ (kg/s), and flash, $\dot{m}_{FEi}$ (kg/s):

$$\dot{m}_D = \sum_{i=1}^{N} \dot{m}_{Di} + \sum_{i=2}^{N} \dot{m}_{FEi} \tag{21}$$

For a generic effect i, the mass flow rate of brine $\dot{m}_{Bi}$ (kg/s) is calculated with Eq. (22):

$$\dot{m}_{Bi} = \dot{m}_{B,i-1} - \dot{m}_{Di} - \dot{m}_{FEi} \tag{22}$$

where $\dot{m}_{B,i-1}$ (kg/s) is the mass flow rate coming from effect $i-1$.

The energy balance applied in each effect is presented in Eq. (23):

$$\begin{aligned}(1-\alpha_{i-1})\dot{m}_{T,i-1}\lambda_{c,i-1} + \dot{m}_{FBi}h''_{Vi} + \dot{m}_{B,i-1}h_{B,i-1} = (1-\alpha_i)\dot{m}_{Ti}h'_{Vi} + \\ \alpha_i\dot{m}_{Ti}h'_{ci} + \dot{m}_F\overline{c}_{p,preh,i}(t_{preh,i} - t_{preh,i+1}) + \dot{m}_{Bi}h_{Bi}\end{aligned} \tag{23}$$

where α (-) is the fraction of vapour condensed in the preheater, $\dot{m}_T$ (kg/s) is the total mass flow rate of vapour produced, λ (kJ/kg) is the specific enthalpy of condensation of water, $\dot{m}_{FB}$ (kg/s) is the mass flow rate of vapour produced by flash in the flashing box, h''_{Vi} (kJ/kg) is the specific enthalpy of condensation of the flashing vapour coming from the flash box, h_B (kJ/kg) is the specific enthalpy of the brine, h'_V (kJ/kg) is the specific enthalpy of vaporization of water, h'_c (kJ/kg) is the specific enthalpy of condensation of water, $\overline{c}_{p,preh}$ (kJ/(kg·°C)) is the average specific heat capacity at constant pressure of the feedwater in the preheater, and t_{preh} (°C) is the temperature of the feedwater entering or exiting the preheater. The superscripts $'$ and $''$ denote conditions in the vapour zone after the demister and in the flashing boxes, respectively.

The energy balance in each preheater is defined by Eq. (24):

$$\dot{m}_F \bar{c}_{p,preh,i}(t_{preh,i} - t_{preh,i+1}) = \alpha_i \dot{m}_{Ti} \lambda'_{Vi} + \alpha_i \dot{m}_{Ti} \bar{c}_{p,BPE,i}(T'_{Vi} - T'_{Vsat,i}) \quad (24)$$

where $\bar{c}_{p,BPE}$ (kJ/(kg·K)) is the average specific heat capacity at constant pressure of the vapour in the vapour zone, T'_V (°C) is the temperature of the vapour, and T'_{Vsat} (°C) is the saturation temperature of the vapour.

Besides, the heat transfer equations associated with the heat exchangers were implemented in the model, such as those correspondents with the heat transfer in each evaporator i, determined by Eq. (25):

$$(1 - \alpha_{i-1}) \dot{m}_{T,i-1} \lambda_{c,i-1} = A_i U_{e,i}(T_{c,i-1} - T_i) \quad (25)$$

where A (m^2) is the heat transfer area of the evaporator, U_e (kJ/kg·K) is the overall heat transfer coefficient of the evaporator, T_c (°C) is the temperature of the condensing steam inside the tubes, and T (°C) is the temperature of the evaporating water on the outer surface of the tubes.

In addition, for each preheater i, the heat transfer equation was considered:

$$\dot{m}_F \bar{c}_{p,preh,i}\left(t_{preh,i} - t_{preh,i+1}\right) = A_{preh,i} U_{preh,i} LMTD_{preh,i} \quad (26)$$

$$LMTD_{preh,i} = \frac{t_{preh,i} - t_{preh,i+1}}{ln\left(\frac{T'_{Vi} - t_{preh,i+1}}{T'_{Vi} - t_{preh,i}}\right)} \quad (27)$$

where A_{preh} (m^2) is the heat transfer area of the preheater, U_e (kJ/kg·K) is the overall heat transfer coefficient of the preheater, and $LMTD_{preh}$ (°C) is the logarithm mean temperature difference in the preheater.

The thermal performance of the MED process can be related to the specific thermal energy consumption sE (kWh/$m^3_{distillate}$):

$$sE = \frac{\dot{m}_s \lambda_s}{\dot{m}_D / \rho_D} \cdot \frac{1}{3600} \quad (28)$$

where $\dot{m}_s$ (kg/s) is the mass flow rate of external steam entering the first evaporator, λ_s (kJ/kg) is the specific enthalpy of condensation of the external steam, and ρ_D (kg/m^3) is the density of the distillate water.

The specific heat transfer area sA (m^2/(kg/s)) of the MED unit is a parameter that accounts for the amount of heat exchanger area required per mass flow rate unit of distillate produced, representing an important share of the total capital costs of the unit:

$$sA = \frac{\sum_{i=1}^{N} A_i + \sum_{i=1}^{N-1} A_{preh,i} + A_c}{\dot{m}_D} \quad (29)$$

where A_c (m^2) is the heat exchanger area of the end condenser.

2.3 Integrated model

The RED and MED units are integrated as presented in Fig. 3. At the outlet of the RED unit, the high concentrated solution has lost mass of salt, which passes to the dilute stream through the membranes. Conversely, the low concentrated solution has gained mass of salt. Therefore, two mixers (Mixer 1 and Mixer 2) are proposed to restore the initial salinity of the solutions, although they consume part of the chemical exergy content of the two streams, reducing the efficiency of the process. In Mixer 1, part of the outlet dilute ($\dot{m}_{bypass}$) is mixed with the outlet concentrate ($\dot{m}_{HC,out}$), restoring the salt lost in the latter through the membranes and decreasing its concentration. In Mixer 2, the distillate produced in the MED unit ($\dot{m}_D$) is mixed with the rest of the dilute solution ($\dot{m}_{LC,M2,in}$) re-establishing the initial dilute concentration ($\dot{m}_{LC,in}$). The MED unit is used as a regeneration stage, rebuilding the initial concentrations of the solutions by evaporating the amount of solvent needed. By applying global mass and salt balances to the mixers and MED unit, the required bypass of dilute flow rate, distillate flow rate and the conversion ratio of the MED process are determined using Eqs. (30)-(34):

$$X_{HC,out}\dot{m}_{HC,out} + X_{LC,out}\dot{m}_{bypass} = X_{MED,in}\dot{m}_{MED,in} \quad (30)$$

$$\dot{m}_{HC,out} + \dot{m}_{bypass} = \dot{m}_{MED,in} \quad (31)$$

$$X_{MED,in}\dot{m}_{MED,in} = X_{HC,in}\dot{m}_{HC,in} \quad (32)$$

$$X_{LC,M2,in}\dot{m}_{LC,M2,in} + X_D\dot{m}_D = X_{LC,in}\dot{m}_{LC,in} \quad (33)$$

$$\dot{m}_{LC,M2,in} + \dot{m}_D = \dot{m}_{LC,in} \quad (34)$$

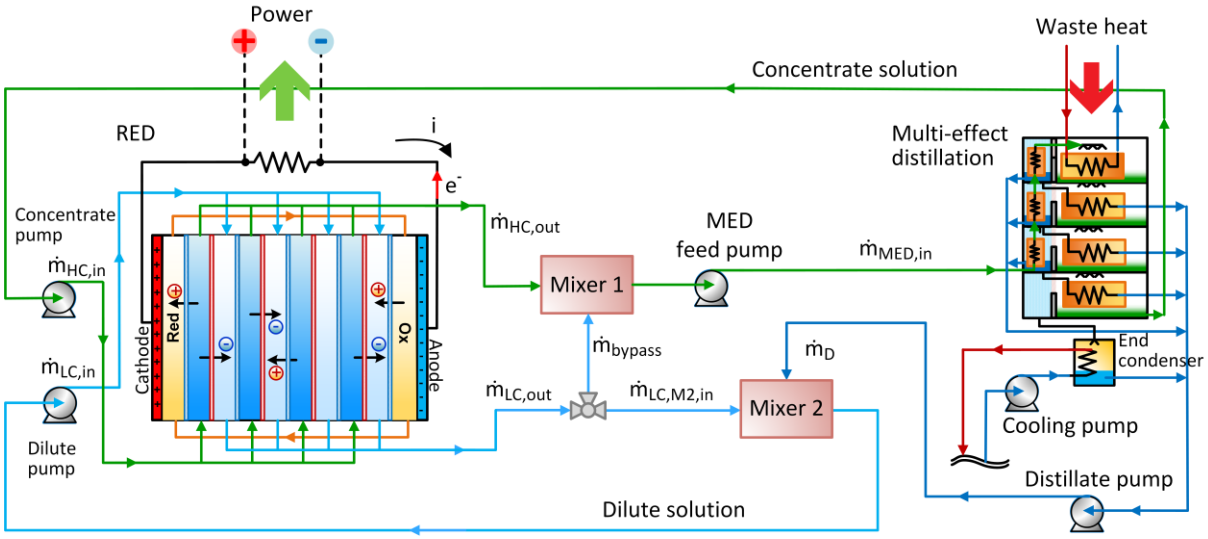

Fig. 3. Scheme of the closed-loop RED-MED HE.

In addition to the mass balance equations, a number of auxiliary equations have been used to estimate the thermodynamic properties of the NaCl-water solution, which is used as the working fluid of the RED-MED HE. The aqueous NaCl solution model, based on the Pitzer's semi-empirical equations [49], has been selected to calculate the activity and osmotic coefficients (see Appendix A). This model is recommended for the chemical exergy evaluation of electrolytic solutions, such as NaCl-water [50]. The specific enthalpy and entropy of the NaCl aqueous solution are tabulated in [49] as a function of the temperature, pressure, and concentration. Correlations have been derived from these data and used in the present model formulation. Other physical properties, namely density, conductivity, diffusivity and viscosity have been also calculated by means of empirical correlations, which are reported in Appendix A.

2.4 Exergy analysis

Exergy analysis is used to identify and quantify sources of internal and external thermodynamic inefficiencies in a system, which are responsible for the loss of work potential [51]. For the RED-MED HE, whose main objective is to generate power using low-grade heat as fuel, the evaluation of the exergy destroyed and lost in each sub-system can help to improve the performance of the whole system. For a thermodynamic system, exergy is defined as the maximum theoretical work obtainable when the system reaches thermal, mechanical and chemical equilibrium with the environment.

If a steady-state flow is considered, the total specific molar flow exergy $\bar{e}_t$ (J/mol) of a system, is given by the sum of the thermomechanical $\bar{e}_{ph}$ and chemical $\bar{e}_{ch}$ contributions:

$$\bar{e}_t = \bar{e}_{ph} + \bar{e}_{ch} \tag{35}$$

which are calculated by Eqs. (36) and (37), respectively:

$$\bar{e}_{ph} = \bar{h} - \bar{h}^* - T_0(\bar{s} - \bar{s}^*) \tag{36}$$

$$\bar{e}_{ch} = \sum_{i=1}^{n} (\mu_i^* - \mu_{0,i}) x_i \tag{37}$$

where $\bar{h}$ (J/mol) and $\bar{s}$ (J/(mol·K)) are the molar enthalpy and entropy of the inlet mixture, the asterisk denotes the restricted dead state, i.e., the system is in thermal and mechanical equilibrium with the environment at T_0, p_0 but with the original composition, x_i the mole fraction of the i^{th}-component, and μ_i (J/mol) the chemical potential of a component i in a solution, given by Eq. (38) [52]:

$$\mu_i = \mu_i^0 + RTln\left(\frac{a_i}{a_i^0}\right) \tag{38}$$

where T (K) is the temperature of the solution, and a_i (-) is the activity of the component i.

The chemical potential of an electrolyte B, μ_B (J/mol), under electrical neutrality, is determined by Eq. (39):

$$\mu_B = \mu_B^0 + \nu RTln(m_{\pm}\gamma_{\pm}) \tag{39}$$

where ν is the total number of ions $(\nu_1 + \nu_2)$, and $m_{\pm}$ and $\gamma_{\pm}$ are the mean molality and mean activity coefficients. For uni-uni (1-1) valent electrolytes, $m_{\pm} = m$. The subscript $\pm$ is habitually removed for simplicity. The chemical potential of the solvent s in the solution, μ_s (J/mol), is evaluated using Eq. (40):

$$\mu_s = \mu_s^0 + RTln(a_s) \tag{40}$$

where a_s (-) is the activity of the solvent, and the subscript "0" denotes the standard or dead state, habitually assumed as the pure solvent at the pressure and temperature of the solution. The activity of the solvent is calculated as a function of the osmotic coefficient ϕ (-) [52]:

$$\phi = \frac{-1000 \cdot ln(a_s)}{M_s \sum_k \nu_k m_k} \tag{41}$$

where M_s (g/mol) is the molar mass of the solvent, ν_k (-) represents the moles of ions in the solution of the electrolyte k, and m_k (mol/kg) is the molality of the electrolyte k.

In the exergy analysis carried out the following assumptions have been made:

- Steady-state operation of the system.
- The kinetic and potential terms in the exergy calculation were neglected.
- In the flow exergy calculation, the physical part of the specific exergy of the solution has been neglected as the NaCl-water streams entering and exiting each component are assumed to be at 25 °C, which is the dead state temperature, and the influence of the pressure variation is much lower than that of the temperature variation, according to [49,53].
- The following dead state has been considered: x_0=38,000 ppm of NaCl, p_0=101,325 Pa, and T_0=25 °C.

2.4.1 Exergy efficiency definition

The exergetic (or exergy) efficiency definition of each component of the system follows the guidelines presented by Tsatsaronis [54]. The product and fuel are described in net terms (exergy increases for the product and exergy decreases for the fuel). The product is considered as the stream of interest (i.e. the useful product), material or energy, for which the system has been designed and conceived. Conversely, the fuel is defined as the exergy flow (i.e. the resource) consumed to generate the desired product. Therefore, the exergy rate of fuel $\dot{E}_F$ (W) for each component *k* and for the overall system are defined by Eq. (42):

$$\dot{E}_{F,k} = \dot{E}_{P,k} + \dot{E}_{D,k} \tag{42}$$

where $\dot{E}_P$ (W) is the exergy rate of the product and $\dot{E}_D$ (W) is the exergy destruction due to irreversibility sources of the system (processes involving temperature differences, pressure drop and dissipative effects, such as friction, viscosity, etc.). Note that for exergy balances on the control volumes, with inlets and outlet streams, of matter or energy, rate of exergy $\dot{E}$ (W) is used. Hereinafter, this variable, calculated as the product of the molar flow rate and the specific molar exergy ($\dot{E} = \dot{N} \cdot \bar{e}_t$), is selected to describe the method and perform the exergetic analysis.

The overall exergetic efficiency η_X (-) is calculated as the ratio of the exergy rate of the product ($\dot{E}_P$) and the exergy rate of the fuel ($\dot{E}_F$):

$$\eta_X = \frac{\dot{E}_P}{\dot{E}_F} \tag{43}$$

Fig. 4a shows the discretization level of the system related to the exergy balance calculation and exergy efficiency definition. The control volumes for each component, for the global system, and the inlet and outlet exergy streams are depicted. Conversely, in Fig. 4b, the functional diagram is presented, which is a dual representation to the physical scheme often adopted in thermoeconomic analysis, in order to clearly identify the fuels and products for each component and the functional interactions among them.

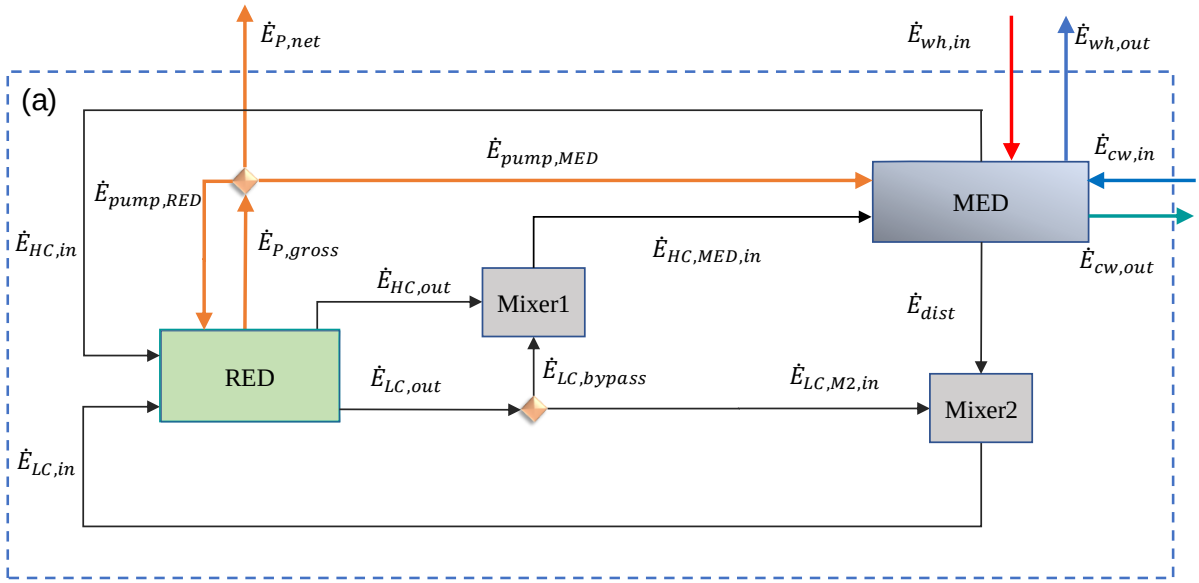

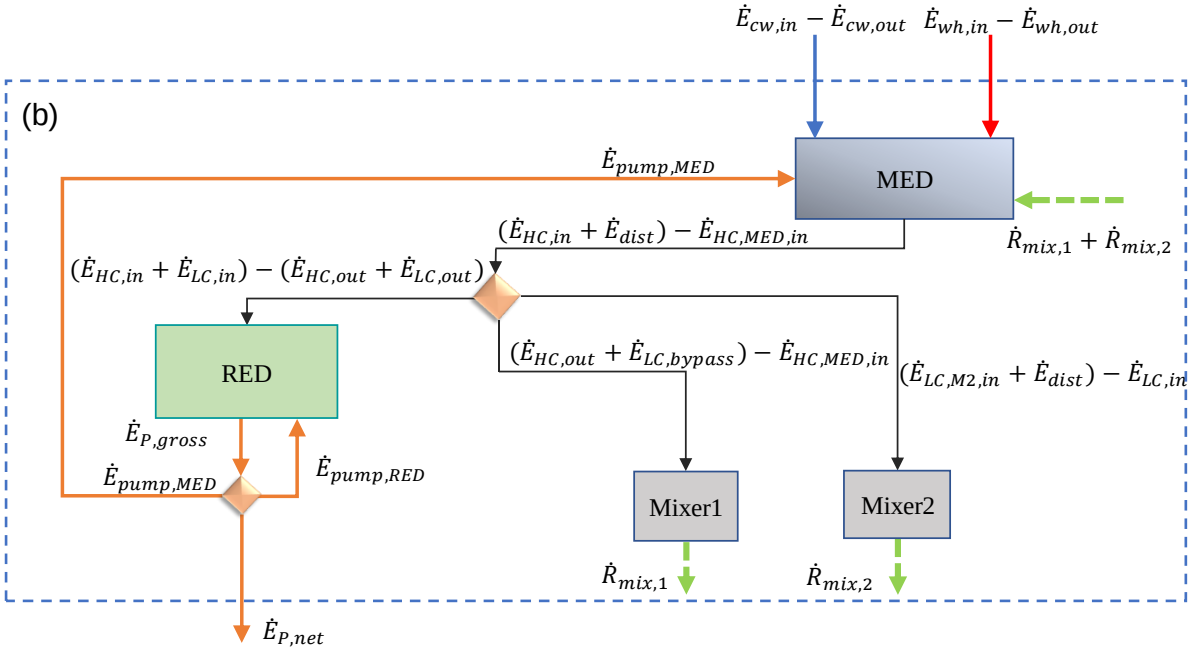

Fig. 4. (a) Schematic representation of exergy flows involved in the closed-loop RED-HE, with each box representing the control volume where the exergy efficiency is calculated (solid line for the components, dashed line for the overall system). (b) Functional diagram of the RED-MED HE depicting fuel-product and residue for each component.

As the purpose of a RED unit is to generate electric power, the product of the RED process in Fig. 4b is the exergy rate of the net electric power produced. It is obtained by subtracting the exergy rate of the RED pumping power consumption, $\dot{E}_{pump,RED}$ (W), to the exergy rate of the gross electric power, $\dot{E}_{P,gross}$ (W), which are equal to the pumping power $P_{pump,RED}$ (W) and gross electric power P_{gross} (W), respectively. On the other hand, the fuel is the rate of exergy decrease of the inlet solutions, i.e., high concentrate solution and low concentrate solution. Therefore, the exergy efficiency of the RED process, $\eta_{X,RED}$ (-), is defined by Eq. (44):

$$\eta_{X,RED} = \frac{\dot{E}_{P,gross} - \dot{E}_{pump,RED}}{\left(\dot{E}_{HC,in} - \dot{E}_{HC,out}\right) + \left(\dot{E}_{LC,in} - \dot{E}_{LC,out}\right)} \tag{44}$$

Both Mixer 1 and Mixer 2 represent sources of irreversibility for the process, however, their presence is necessary for the operation of the system. From a fuel-product perspective, these components lack productive purposes, and they are often identified as dissipative units [55]. The amount of exergy destroyed represents their fictitious product and it is usually named residue exergy flow $\dot{R}$ (indicated by the green dotted line in Fig. 4b). Following a well-established criterion proposed in [56], these flows are allocated as additional fuels to the component that contributed to their formation process, i.e. the MED unit (see Fig. 4b). The functional diagram presented above is just provided for the sake of completeness, in order to clarify the rational approach adopted in the definition of exergy efficiency for each individual component. However, no further details are given as the aim of this work is to perform an exergy analysis and is not related to a thermoeconomic cost estimation. The reader is invited to refer to the cited references for more information.

In order to account for the amount of exergy destroyed in the mixers, due to the absence of a useful product measurable in exergy units, the exergy efficiencies of Mixer 1 ($\eta_{X,M1}$) and Mixer 2 ($\eta_{X,M2}$) were determined according to Eqs. (45) and (46), respectively:

$$\eta_{X,M1} = \frac{\dot{E}_{HC,MED,in}}{\dot{E}_{HC,out} + \dot{E}_{LC,bypass}} \quad (45)$$

$$\eta_{X,M2} = \frac{\dot{E}_{LC,in}}{\dot{E}_{dist} + \dot{E}_{LC,M2,in}} \quad (46)$$

The MED unit is used to restore the initial concentration and flow rate of the concentrate solution, before entering in the RED unit. This component uses external heat for the thermal separation of the solute and the solvent, both with higher exergy than the feed stream. Therefore, referring to Fig. 4b, the product of this subsystem is defined as the increase of the exergy content of the outlet material streams (concentrate and distillate) with respect to the inlet stream. The fuel is defined as the sum of the exergy content of the waste heat added to the MED, the cooling water and the pumping power. Therefore, the exergy efficiency of the MED process $\eta_{X,MED}$ (-) is defined by Eq. (47):

$$\eta_{X,MED} = \frac{\dot{E}_{HC,in} + \dot{E}_{dist} - \dot{E}_{HC,MED,in}}{\dot{E}_{wh,in} - \dot{E}_{wh,out} + \dot{E}_{cw,in} - \dot{E}_{cw,out} + \dot{E}_{pump,MED}} \quad (47)$$

In exergy analyses of the MED process is not common to include the exergy flow of the cooling water when defining the global exergy performance [57]. For the examined case, as shown in Eq. (47), the exergy of the cooling water supplied to the condenser of the MED unit is considered an additional fuel of the overall system. The RED-MED HE interacts with three thermal sources: the waste heat source (100 °C), the river water in the condenser (15°C) and the environment (25°C). The authors decided to use the air temperature as the temperature of the dead state since it is assumed that all the system components except the MED unit operate in thermal equilibrium with the surrounding air. Stemming from this assumption, the thermal exergy content of the cooling water taken from a river (considered as an additional exergy quantity used as a fuel) equals the theoretical work of a reversible heat engine operated between the temperature of the river water (assumed equal to 288.15 K) and the air temperature (T_0=298.15 K).

The global exergy efficiency $\eta_{X,g}$ (-) of the RED-MED HE is defined as the ratio between the exergy content of the net electric power produced by the RED unit and the sum of the exergy content of the waste heat supplied to the MED unit ($\dot{E}_{wh,in} - \dot{E}_{wh,out}$) and the exergy added by the cooling water ($\dot{E}_{cw,in} - \dot{E}_{cw,out}$), as reported in Eq. (48):

$$\eta_{X,g} = \frac{\dot{E}_{P,gross} - \dot{E}_{pump,RED} - \dot{E}_{pump,MED}}{\dot{E}_{wh,in} - \dot{E}_{wh,out} + \dot{E}_{cw,in} - \dot{E}_{cw,out}} \quad (48)$$

The exergy produced by the RED unit is equal to the gross power produced, $\dot{E}_{P,gross}$, minus the pumping power required by the RED and MED units, $\dot{E}_{pump,RED}$ and $\dot{E}_{pump,MED}$. Due to the higher requirements of the MED pumping, this term will particularly affect the global performance of the system.

The thermal efficiency of the overall system $\eta_{th,g}$ (-) is calculated with Eq. (49):

$$\eta_{th,g} = \frac{P_{gross} - P_{pump,RED} - P_{pump,MED}}{\dot{Q}_{wh,in} - \dot{Q}_{wh,out}} = \frac{P_{net}}{\dot{m}_{wh} \cdot \Delta h_{cond}} \quad (49)$$

where P_{net} (W) is the net power produced, $\dot{Q}_{wh}$ (W) is the waste heat rate, assumed to be in saturation conditions, $\dot{m}_{wh}$ (kg/s) is the mass flow rate of the waste heat, and Δh_{cond} (J/kg) is the specific enthalpy of condensation.

2.5 Solving structure

The structure of the solving algorithm used in EES is depicted in Fig. 5. Firstly, the RED and MED inputs are introduced in the simulation tool. After that, the equations with a single unknown variable are solved. All variables are then initialized and the iteration procedure is started. EES solves numerically non-linear equation systems using Newton's method and properly blocking and reordering the equations in order to efficiently find the value of each variable. The stopping criterion usually is the relative residual for each equation. When all the residuals are below a certain tolerance ϵ, the iterations finish, otherwise, the variables are updated to their last values and a new iteration is started. After solving, the effective temperature difference is evaluated. If it is lower than the minimum required, the number of effects are decreased. Also, there is an optional optimization step to obtain the maximum performance of the system by varying the external load, in this case, the algorithm is repeated for values of external load resistance until maximum efficiency is achieved. Finally, the results are obtained.

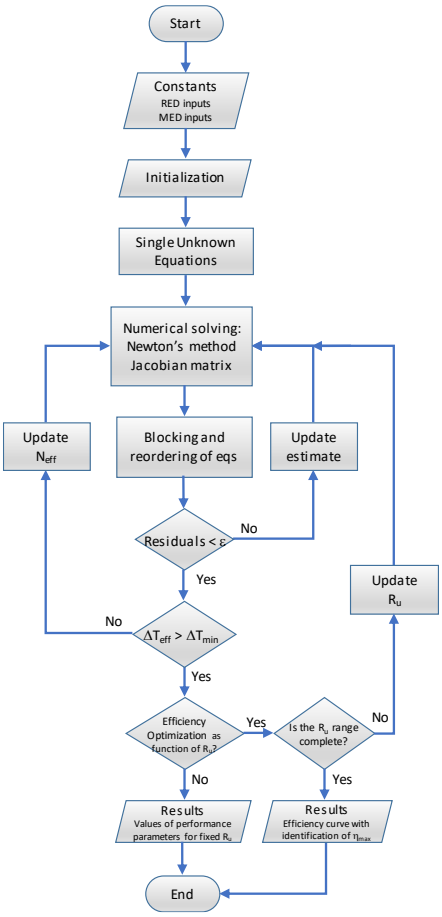

Fig. 5. Schematic of the solving structure used in EES.

2.6 Simulation scenarios

The methods followed in this work to investigate the performance potential and the exergy destruction sources of the RED-MED HE are presented hereafter, where the integrated model described in the previous section is used to carry out the simulations (reported in Section 4).

2.6.1 Reference case

As a first step, a reference case is chosen to quantify the exergy performance of the system under common design and operating conditions. This scenario will be compared later on with the one obtained after carrying out the different sensitivity analyses, selecting the best performing conditions found for each case. The reference case selected considers a RED unit of 1000 cell pairs, a membrane area of 0.25 m × 1 m (width – length), counter-current flow arrangement, inlet solutions concentrations and velocities of 3 – 0.05 M and 1 – 1 cm/s for the concentrate and dilute solutions, respectively. The electrical operating point of the RED unit has been chosen in order to maximise the exergy efficiency of the RED subsystem (according

to the exergy efficiency curve shown in Fig. 6a in the next section). The properties of the IEMs have been provided by Fujifilm (reference membrane properties, Appendix A). The rest of the input variables for the RED and MED units are presented in Table 1. The number of cell pairs has been considered high enough to neglect the effect of the blank resistance (electrodes compartments). In addition, the number of MED effects selected is limited by the inlet solutions concentration and velocity (high boiling point elevation).

Table 1. Main RED-MED HE model inputs for the reference case.

Concept	**Value**
RED UNIT	
Cell pair	
Flow pattern, (-)	Counter-current
Number of cell pairs, (-)	1000
Width, b (m)	0.25
Length, L (m)	1
Blank resistance, R_{blank} ($\Omega \cdot m^2$)	3.27×10^{-3}
Operation temperature, T (°C)	25
Solutions	
Concentrate inlet concentration, C_{HC} (mol/L)	3
Dilute inlet concentration, C_{LC} (mol/L)	0.05
Inlet concentrate velocity, v_{HC} (cm/s)	1
Inlet dilute velocity, v_{LC} (cm/s)	1
Membranes (Fujifilm Type 10)	
Thickness, δ_m (m)	1.25×10^{-4}
Water permeability[a], P_w (m/(Pa·s))	2.22×10^{-14}
Salt permeability coefficient[a], P_s (m^2/s)	4.52×10^{-12}
Permselectivity, α (-)	Appendix A
Electrical resistance, R_{IEM} ($\Omega \cdot cm^2$)	Appendix A
Spacer (Deukum)	
Concentrate spacer thickness, δ_{HC} (m)	1.5×10^{-4}
Dilute spacer thickness, δ_{LC} (m)	1.5×10^{-4}
Relative concentrate spacer volume, ϵ_H (-)	0.175
Relative dilute spacer volume, ϵ_L (-)	0.175
Shadow factor, s_f (-)	1.563
MED UNIT	
Number of effects[b], (-)	24
Heating steam temperature, (°C)	100
Last effect temperature, (°C)	27
Terminal temp. difference preheater 1, (°C)	3
Terminal temp. difference end condenser, (°C)	3
Intake cooling water temperature, (°C)	15
Evaporators tube bundle	L: 1 m; diam.: 22 mm
End condenser tube bundle	L: 2 m; diam.: 25 mm

PUMPS	
Pumps efficiency, η_p (-)	0.8

[a] Properties provided by Fujifilm Manufacturing Europe B.V.
[b] The number of effects is intrinsically related to the effective temperature driving force in each effect, which has an average value of 1°C for the reference case.

2.6.2 Effect of irreversibility sources

The irreversibility sources of the RED-MED HE are identified and quantified, extending the previous work performed in [29], where several detrimental effects on the performance of the RED unit were investigated: the ohmic losses due to the internal resistance of the stack, the membrane permselectivity, the diffusive salt flux and the water osmotic flux across the IEMs. Here, the analysis considers four additional scenarios: polarization phenomena, RED pumping consumption, MED pumping consumption, and the effective temperature driving force (i.e. the difference between condensing vapour and evaporating brine temperature) in each effect of the MED unit.

For this analysis, the same inputs as the reference case have been taken (0.25 m × 1 m, 3 – 0.05 M, 1 – 1 cm/s), and the number of MED effects have been selected in order to adapt to the concentration factor (or recovery ratio) required, while maintaining an effective temperature driving force between 1 – 2 °C (except in case H, where it is varied). In each of the eight scenarios analysed, one effect per time has been added, starting from an ideal condition (where only internal ohmic losses in the RED unit and the heat transfer losses in the MED are considered) and eventually including all the identified sources of irreversibility in the final scenario, as described below:

- Scenario A. Ideal case, where only the internal ohmic losses are considered (ideal membrane properties): P_w=0 m/(Pa·s), P_s=0 m^2/s, θ_H= θ_L=1, and α=1.
- Scenario B. The effect of the non-ideal permselectivity of the membranes is taken into account: P_w=0 m/(Pa·s), P_s=0 m^2/s, θ_H= θ_L=1, and $\alpha\neq1$.
- Scenario C. In this case both the non-ideal permselectivity and diffusive salt flux are added: P_w=0 m/(Pa·s), P_s=10^{-12} m^2/s, θ_H= θ_L=1, and $\alpha\neq1$.
- Scenario D. This case adds the water flux: P_w=2.22×10^{-14} m/(Pa·s), P_s=10^{-12} m^2/s, θ_H= θ_L=1, and $\alpha\neq1$.
- Scenario E. The polarization effect is included in this scenario: P_w=2.22×10^{-14} m/(Pa·s), P_s=10^{-12} m^2/s, $\theta_H\neq1$, $\theta_L\neq1$, and $\alpha\neq1$.

- Scenario F. In this case, the pumping power consumption of the RED unit (concentrate and dilute solution pumps) is considered.
- Scenario G. The pumping power consumption of the MED unit (feedwater, concentrate, distillate and cooling pumps) is accounted.
- Scenario H. The mean effective temperature difference driving force in each effect of the MED unit is fixed equal to 5.5 °C.

2.6.3 Sensitivity analyses

After the evaluation of the irreversibility sources of the RED-MED HE, sensitivity analyses of the exergy efficiency of the overall RED-MED system and each component (RED unit, MED unit, Mixer 1 and Mixer 2) have been carried out, as a function of the main operating and design variables. The effect on the performance of the inlet solutions concentration and velocity, together with the membrane's aspect ratio, has been investigated starting from a general reference case. On-design analyses for different design schemes have been selected, specifying the dimensions of the RED membranes and MED effects. Finally, the same sensitivity analyses are performed using high-performing membranes (IEMs with improved features), in order to provide insights into the real exergy potential of the RED-MED HE technology.

3. RESULTS AND DISCUSSION

Results for the quantification of the irreversibility sources of the RED-MED HE system are presented, starting from a reference case. Also, results for the sensitivity analyses of the exergy and thermal efficiency as a function of the main operating and design parameters are reported, at global and component level.

3.1 Reference case

Table 2 shows the main results obtained after simulating the reference case. The low values of the exergy and thermal efficiencies (2.3% and 0.5%, respectively) are mainly due to the irreversibility sources associated with poor membrane properties, as it will be discussed in next sections. The exergy efficiency of the RED unit, about 18%, is low compared to the one of the MED unit, which reaches a relatively high performance, around 37%. Mixer 1 and Mixer 2 have exergy efficiencies equal to 76.9% and 78.6%, respectively, suggesting that the exergy

destruction in these components is low under the considered conditions. Related to the pumping power consumption, the MED unit consumes much more power than the RED unit, 273.7 W against 25.6 W, respectively, mainly due to the higher pressure drop occurring within the MED unit.

Table 2. Results for the reference case.

Concept	Value
Global exergy efficiency, $\eta_{X,g}$ (%)	2.3
Global thermal efficiency, $\eta_{th,g}$ (%)	0.5
RED exergy efficiency, $\eta_{X,RED}$ (%)	17.7
MED exergy efficiency, $\eta_{X,MED}$ (%)	37
Mixer 1 exergy efficiency, $\eta_{X,M1}$ (%)	76.9
Mixer 2 exergy efficiency, $\eta_{X,M2}$ (%)	78.6
Gross power, P_{gross} (W)	487.2
RED pumping power, $P_{pump,RED}$ (W)	25.6
MED pumping power, $P_{pump,MED}$ (W)	273.7
Waste heat rate, $\dot{Q}_{wh}$ (kW)	37

3.2 Effect of irreversibility sources

The trends for RED exergy efficiency as a function of the electric current are shown in Fig. 6a. For short-circuit conditions (maximum current, external resistance approaching zero) the global exergy efficiency is null as the electro-motive force is entirely dissipated inside the pile. Considering only the ohmic losses due to the internal resistance (scenario A), when the electric current decreases the exergy efficiency increases, reaching a value of ~100% for open circuit voltage (OCV) conditions (null electric current, the stack voltage is equal to the electro-motive force), where the process approaches reversibility. When the permselectivity is also taken into account (scenario B), the same trend is followed and the highest exergy efficiency (84%) is lower than the previous case due to a reduction in the electro-motive force (Eq. (1)).

The diffusive salt flux and osmotic water flux (scenarios C and D) significantly change the trend of the RED exergy efficiency to a bell shape, increasing when the current decreases until reaching a maximum (35.7% and 19.1%, respectively) for currents between 6 – 10 A. Below these values a reduction on the performance is observed due to the dissipative mixing phenomena becoming more important than the migrative flux of ions, eventually leading to a null value of the efficiency in OCV condition. Polarization phenomena (scenario E), reducing

the effective driving force in the RED process, decrease only slightly the RED exergy efficiency. Finally, as expected, the irreversibilities due to the MED pumping and temperature driving force (scenarios G and H) do not have any effect on the RED exergy efficiency.

The effect of the electric current on the exergy efficiency of Mixer 1 is depicted in Fig. 6b. The exergy destruction in Mixer 1 is determined not only by the amount of salt transferred in the RED unit, which has to be restored in the concentrate loop, but also by the outlet concentration of the dilute solution, both affecting the by-pass flow rate. When high salt flux in the RED unit (Eq. (12)) is achieved (i.e. high current and/or high diffusive flux), the amount of the salt exchanged in the RED unit increases (Fig. 7a), leading to an increase in the need of salt restoring in the concentrate loop. This is, however, made easier by the high concentration in the dilute solution to be by-passed (Fig. 7b). Conversely, when the salt flux is low (e.g. low diffusion and electric current, approaching OCV conditions), a small salt restoring has to be guaranteed. However, in this case, the dilute concentration is very low, thus requiring a large volume of by-pass solution to restore the even small amount of salt to the concentrate loop. The large concentration difference leads to a larger exergy dissipation due to the mixing.

When ideal membranes are considered (Fig. 6b), exergy efficiency starts from 100% at zero current, rapidly goes down to a minimum, and then increases with the current. When non-idealities are considered (i.e. diffusive salt flux), salt passage is observed also at zero current and the minimum efficiency is observed at this point, while an increase in current leads to the enhancement of exergy efficiency tending to 100% in the not-always possible condition of equal dilute-concentrate concentration.

The effect of the electrical current on the exergy efficiency of the MED is depicted in Fig. 6c. From short-circuit conditions (maximum electric current) up to ~2 A, its efficiency is almost constant (~38% for scenarios A-F) because the concentration regeneration requirements only change slightly. When current values below 2 A are considered, a fast drop in the MED efficiency is observed for cases A and B, where the salinity profile in the RED unit is conserved (see Fig. 7a) due to the absence of uncontrolled mixing of salt and water fluxes. In those cases, the solutions regeneration requirement is very low, hence a lower number of MED effects are used. For the rest of the cases, the concentration of the solutions at the exit of the RED unit are different and higher regeneration requirements are needed. Therefore, the number of MED effects is kept constant and the exergy efficiency undergoes only a slight increase. When the MED pumping consumption is taken into account (scenario G), the exergy efficiency decreases approximately one percentage point, due to the lower value of the pumping power in comparison with the thermal energy required. Finally, if a mean effective temperature

difference at the MED unit of ~5.5 °C is considered (scenario H), the efficiency decreases up to 18%, as the number of effects is reduced from 24 to 10, and more waste heat is needed in the regeneration stage.

Regarding the effect on the exergy efficiency of Mixer 2 (Fig. 6d), for all the cases, its value increases when approaching to OCV condition. In fact, when reducing the ionic current in the pile, a lower variation in the concentration of both solutions within the RED unit is observed. This fact eventually leads to the reduction of the amount of distillate flow rate separated by the MED unit, which is then mixed in Mixer 2. In particular, for scenarios A and B, where no uncontrolled mixed phenomena occur, the exergy efficiency reaches ~100% in short-circuit conditions, since no distillate mixing is needed to restore the initial concentration of the dilute solution.

The effect of the electrical current on the global exergy efficiency is presented in Fig. 6e, where a maximum (2.3%) is found for a current of ~10 A, as a result of the combined effect of each component. There is a significant decrease associated to the non-ideal permselectivity of the membranes (passing from 13.2% in case A to around 9.5% in case B), the uncontrolled mixing phenomena related to the permeability to the diffusive salt flux (7.8% in case C), the osmotic water flux (6% case D), and the pumping power consumption in the MED unit linked to the pressure drop (from 5.5% of case F to 2.3% of case G).

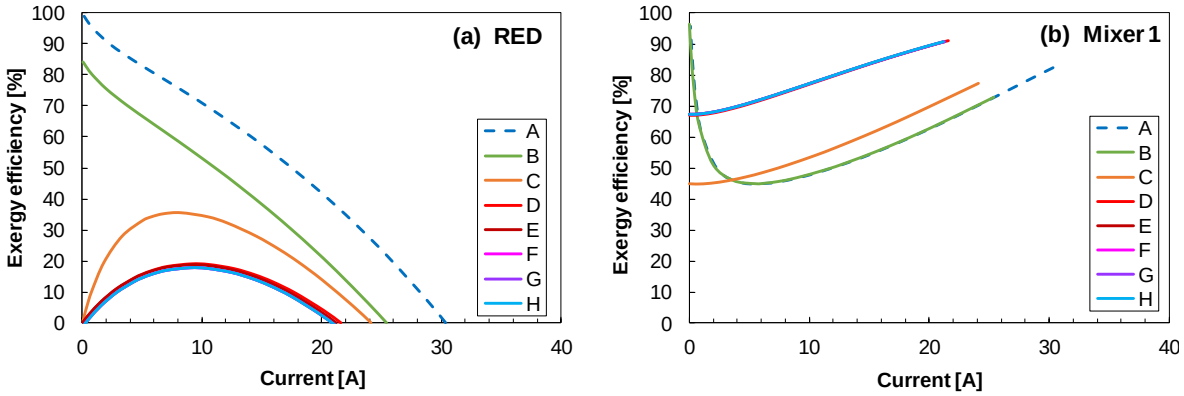

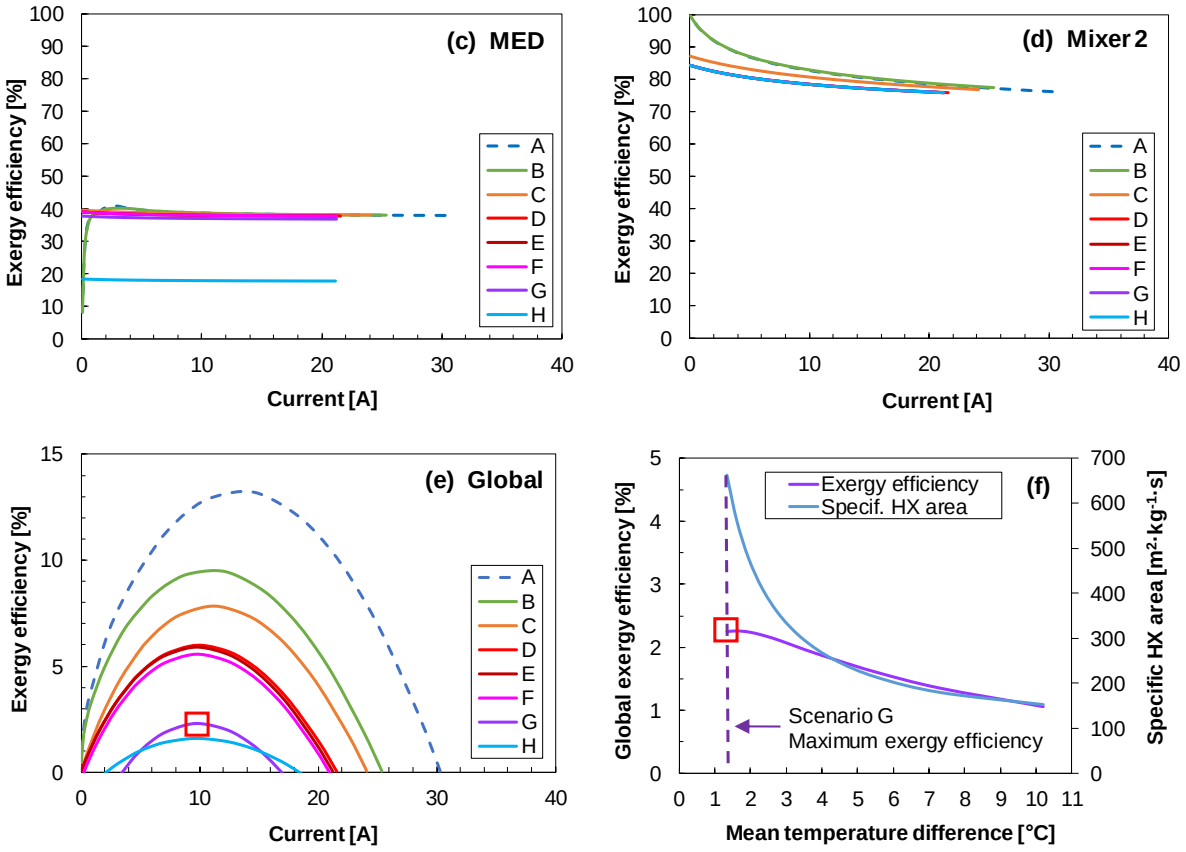

Fig. 6. Exergy efficiency as a function of the electric current and the irreversibility sources, in the reference case: (a) RED, (b) Mixer 1, (c) MED, (d) Mixer 2, and (e) Global. (f) Global exergy efficiency and specific heat transfer area as a function of the mean effective temperature difference of the MED unit (scenario G).

Finally, Fig. 6f presents the influence of the mean effective temperature driving force of the MED unit on the global exergy efficiency and the specific heat transfer area, within scenario G conditions and imposing an electrical current (or equivalently an external resistance) leading to maximum performance. In these conditions, increasing the temperature difference from ~1.3 to 10 °C reduces the efficiency from 2.3% to ~1%. However, a lower number of effects can be used (passing from 24 to 6) and a decrease in the specific heat transfer area is observed (from ~650 to 150 $m^2 \cdot kg^{-1} \cdot s$). This fact could be very attractive from an economic point of view, as the heat exchangers represent an important share of the total MED capital costs.

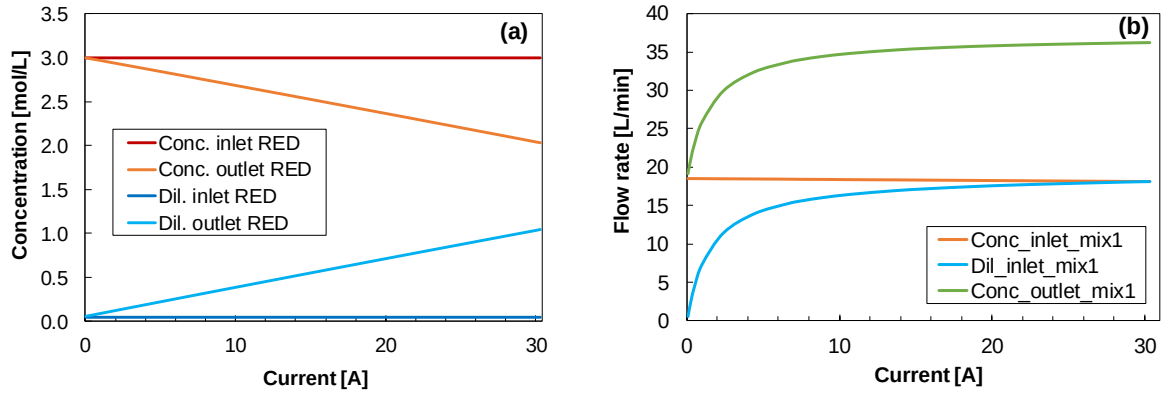

Fig. 7. Inlet and outlet (a) concentration and (b) molar flow rate in the RED unit as a function of the electric current, for scenario A (only internal resistance losses).

3.3 Sensitivity analysis with reference membrane properties

Results for the sensitivity analyses using reference IEMs are shown hereafter, in order to investigate the effect of the main operating and design conditions on the performance of the overall process and components.

3.3.1 Effect of solutions concentration

The component and global exergy efficiency are analysed when the inlet concentrations vary between 2 – 5 M (concentrate) and 0.01 – 0.1 M (dilute), with the rest of parameters being constant as in the reference case, except the number of MED effects, which has been varied in order to keep at least 1 °C of mean effective temperature driving force in each effect. Only the results of the parametric evaluation for the overall RED-MED system are depicted in Fig. 8. The figures for each component (RED unit, MED unit, Mixer 1 and Mixer 2) are reported in the Supplementary Information file, for the sake of brevity.

The exergy efficiency of the RED unit increases for lower values of the concentrate solution salinity, reaching almost 28% at C_{HC}=2 M, while it is not affected by the dilute solution salinity in the range analysed. Lower salinity gradient implies lower power output, however, this behaviour is explained by the lower exergy destruction associated to the uncontrolled mixing phenomena when the concentration difference is reduced [29]. For the MED unit, the exergy efficiency increases up to 55% with the salinity of the concentrate solution, with the maximum at 5 – 0.1 M. Higher concentrations of the concentrate solution reduces the number of effects (due to higher BPEs), but at the same time the exergy difference between the exiting and

entering solutions is larger, therefore, the exergy efficiency rises. The exergetic performance of Mixer 1, defined by Eq. (45), is also favoured by the salinity increase of the inlet concentrate solution, leading to values near 80% at 5 – 0.1 M. On the contrary, the exergy efficiency of Mixer 2, defined by Eq. (46) increases up to ~95% with the decrease of the inlet dilute solution concentration, at 0.01 M. Finally, due to the combination of the different mentioned effects, a maximum global exergy efficiency of 2.1% is reached at an intermediate inlet concentrate solution salinity, 4 – 0.01 M, and 21 MED effects (Fig. 8).

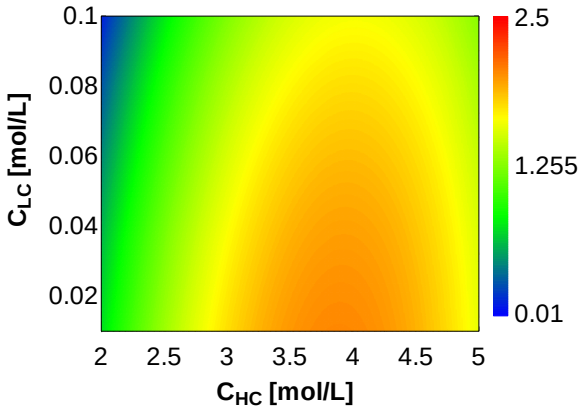

Fig. 8. Global exergy efficiency as a function of the concentrate and dilute inlet concentrations to the RED unit, using reference membranes.

3.3.2 Effect of solutions velocity

The effect of the concentrate and dilute solutions velocity on the exergy efficiency are investigated in the ranges 0.2 – 2 cm/s (HC solution) and 0.5 – 2 cm/s (LC solution). The inlet concentration values are selected as those leading to the maximum performance obtained in the previous analysis (4 – 0.01 M), with the rest of the parameters being constant (except the number of MED effects, changed as described in the preceding section). The figures related to each component are depicted in the Supplementary Information file.

The exergy efficiency of the RED unit is increased for lower values of the inlet concentrate solution velocity and higher values of the dilute solution velocity, reaching a maximum of 25.3% for 0.2 – 2 cm/s ($v_{HC} - v_{LC}$). The first result is due to the reduction of the uncontrolled mixing phenomena (caused by a decrease in the concentration when the residence time is enlarged). On the contrary, the second effect can be attributed to the lower concentration of the dilute solution when its residence time decreases, which enhances the induced voltage (see Eq. (1)).

The exergy efficiency of the MED increases with the concentrate velocity and decreases with the dilute velocity, due to the higher concentration and flow rate of the feed water (RED exiting concentrate solution) obtained in those conditions. The inlet specific exergy is increased more than the heat rate, while the outlet flow exergy of the concentrate and distillate streams remains equal. The maximum value, 48%, is obtained for 2 – 1.5 cm/s.

The exergy efficiency of Mixer 1 follows the same trend as the one observed for the MED. More specifically, the higher the concentration and flow rate of the inlet streams, the higher the exergy efficiency (reaching ~100% for 2 – 0.2 cm/s), which means lower exergy destruction. On the contrary, Mixer 2 is not affected by the velocity of the concentrate solution, and only the dilute solution velocity has a slight influence on the exergy efficiency. Therefore, it is maintained almost constant for all the range of velocities analysed, with a maximum of 95.5% for 0.2 – 2 cm/s.

Finally, the global exergy efficiency (see Fig. 9) results as a combination of the exergy efficiency of all the components. The maximum global exergy efficiency (3.6%) is reached for values of the concentrate and dilute solutions velocity of 0.2 – 0.5 cm/s, respectively, and 26 MED effects, with the thermal efficiency equal to 0.73%.

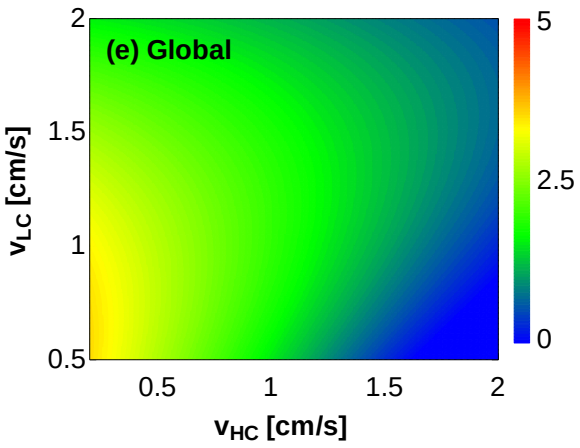

Fig. 9. Global exergy efficiency as a function of the concentrate and dilute inlet velocities to the RED unit, using reference membranes.

3.3.3 Effect of the RED unit aspect ratio

The effect of the RED unit's aspect ratio (length-to-width ratio) on the global exergy efficiency is also analysed. The concentration and velocity of the concentrate and dilute solutions leading to the maximum exergy efficiency have been selected (4 – 0.01 M and 0.2 –

0.5 cm/s, of the HC – LC solutions, respectively). Besides, a constant membrane's area of 0.25 m^2 is assumed.

Increasing the length of the membrane involves higher residence time of the solutions and therefore higher power output, but at the same time the uncontrolled mixing phenomena (salt diffusive flux and osmotic water flux) increases. Overall, Fig. 10 shows the evolution of the global exergy efficiency. A value of R_{geom}=1 (b=0.5 m, L=0.5 m), with 26 MED effects, provides the maximum performance, 4.3% (0.96% thermal), slightly higher than the one found in the solutions velocity analysis (3.6%). This may be explained considering that the increase of the channel length (L) extends the residence time of the solutions, which has been already enhanced in the velocity analysis. Therefore, the analysis of the aspect ratio, once the solutions velocity have been analysed, does not lead to significant higher exergy efficiency for the RED-MED HE.

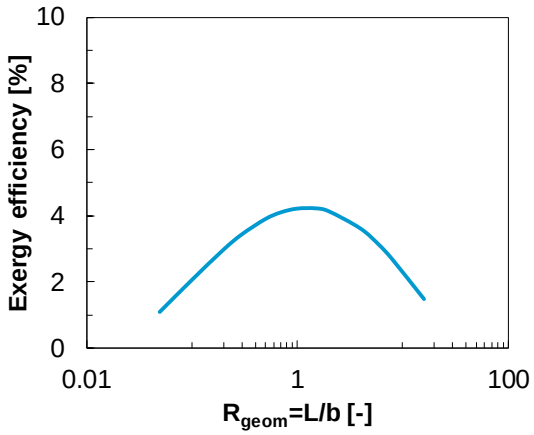

Fig. 10. Global exergy efficiency as a function of the length-to-width (R_{geom}) membrane's aspect ratio, using reference membranes.

3.4 Sensitivity analysis with high-performing membranes

The membrane properties significantly affect the performance of the RED-HE system, as non-ideal phenomena (e.g. permselectivity, salt diffusive flux, water diffusive flux) and ohmic losses (linked to IEMs resistance) are sources of irreversibility that consume part of the total exergy available in the initial salinity gradient. Therefore, in order to improve the overall exergy efficiency of the heat engine, membranes with enhanced features are required.

The exergy efficiency of the system equipped with high-performing IEMs is analysed hereafter. The permselectivity is assumed to be constant and equal to 95% at any concentration,

and the membrane's resistance, salt diffusive flux, and water diffusive flux, are decreased to one fourth of the reference membrane values, which leads to better performance still being a realistic choice of parameters values (as indicated in Fig. A.1 in Appendix A).

The trend of the exergetic efficiency for each component is similar to those explained in the reference membrane's case. However, due to the mitigation of the uncontrolled mixing phenomena and the constant value selected for the permselectivity, the efficiencies are less affected by the variation of the salinity gradient and membranes properties. For the sake of brevity, only the global exergy efficiency is shown in Fig. 11, the analyses for the rest of the components are reported in the Supplementary Information file. The analysis of the inlet concentrations (depicted in Fig. 11a) leads to a maximum global exergy efficiency of 18.2% for 4.5 – 0.01 M and 19 MED effects, while the inlet velocities analysis (Fig. 11b) determines a maximum efficiency of 23.6% for 0.2 – 0.36 cm/s and 23 MED effects. Finally, the evaluation of the membrane's aspect ratio (Fig. 11c) increases the exergy efficiency only marginally to 23.8% (5.4% thermal) for R_{geom}=2.5 (b=0.316 m, L=0.791 m) and 23 MED effects.

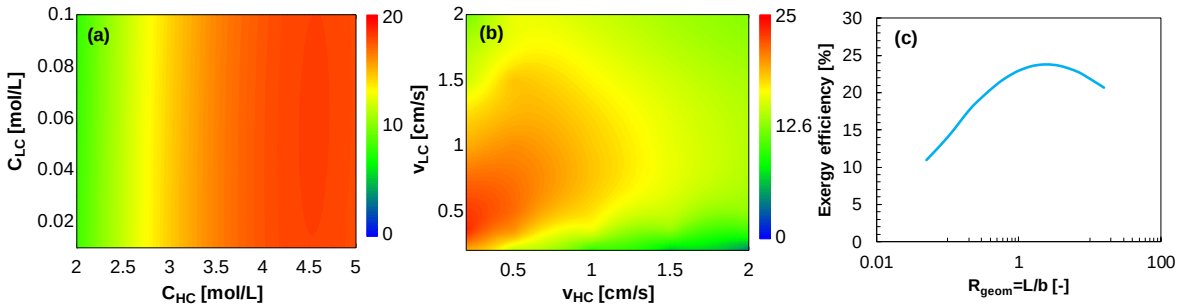

Fig. 11. Global exergy efficiency as a function of the solutions (a) concentration, (b) velocity and (c) stack's aspect ratio, using high-performing membranes.

3.5 Comparative analysis

Table 3 presents a summary of the overall improvement of the RED-MED HE exergy efficiency, after the parametric analyses carried out on the inlet solutions concentration, velocity and membrane's aspect ratio. Particularly, the results for the base case, reference membranes, and high-performing membranes are compared. Results show the great improvement achieved in the performance with respect to the reference case by varying only the operating conditions. The overall exergy efficiency has almost doubled from 2.3% to 4.3%, showing that it is largely affected by the RED process, where a significant amount of exergy destruction occurs. Higher

efficiency is observed by reducing the dilute solution concentration (from 0.05 M to 0.01 M), increasing the concentrate solution concentration (from 3 M to 4 M), and reducing the concentrate solution residence time. Concerning the membrane's aspect ratio, asymmetric membranes with an aspect ratio between 1 and 3 results in the highest performance, under the investigated conditions.

The adoption of high-performing membranes in the RED unit leads to a huge increase in the system efficiency, passing from 4.3% to 23.8%. This is mainly due to the improvement of the IEMs properties and subsequent reduction of the irreversibility sources, which are the main limiting factor of this technology. The RED exergy efficiency reaches 54.9%, while in the base case was only 17.7%, i.e., a three-fold increment. The proper selection of the operation point and the use of high-performing membranes allowed to decrease the irreversibility sources within the RED unit. The MED exergy efficiency increases from 37% to 47.7%, caused by the decrease in the waste heat requirement. Comparing the exergy efficiency of Mixer 1, it is increased from 76.9% to almost 100%, while in the case of Mixer 2 it is raised from 78.6% to 92.3% (the reduction of the outlet dilute concentration enhances the exergy efficiency of Mixer 2). The component with a higher contribution to the exergy destruction of the RED-MED HE in all cases is the MED unit, followed by the RED unit, and the mixers. Besides, more power is generated, 1080 W against the initial 487.2 W, while the heat rate input decreases from 37 to ~18 kW. The specific thermal energy consumption of the MED does not vary significantly (around 35 kWh/m^3) because the decrease in the distillate flow rate is similar to that one of the waste heat steam (approximately one half). This value is found much lower than that of the MD regeneration process for RED-HE applications reported in [27] (> 100 kWh/m^3) and in the range of the most-performing schemes (hybrid MED and adsorption process) in seawater desalination applications (30 – 40 kWh/m^3 reported in [58]).

Table 3. Comparison of the RED-MED HE performance between the reference case and the two best cases analysed with reference and enhanced membranes properties.

Concept	**Base case**	**Reference memb.**	**High-perf. memb.**
Input variables			
Inlet concentrations, (mol/L)	3 – 0.05	4 – 0.01	4.5 – 0.01
Inlet velocities, (cm/s)	1 – 1	0.2 – 0.5	0.2 – 0.36
Membrane aspect ratio, (m × m)	0.25 × 1	0.5 × 0.5	0.316 × 0.791
Number of MED effects	24	26	23
Mean temp. difference, (°C)	1.3	1.2	1
Results			
Exergy efficiency, η_X (%)			

Global	2.3	4.3	23.8
RED	17.7	18.3	54.9
MED	37	39.9	47.7
Mixer 1	76.9	62.2	99.9
Mixer 2	78.6	93.5	92.3
Exergy destruction, $\dot{E}_D$ (W)			
Global	8142	7585	3112
RED	2144	2449	887
MED	5423	4888	2191
Mixer 1	384	187	0.1
Mixer 2	191	61	34
Thermal efficiency, η_{th} (%)	0.51	0.96	5.4
Gross power, P_{gross} (W)	487.8	551.9	1080
RED pumping power, $P_{pump,RED}$ (W)	25.6	3.1	2.2
MED pumping power, $P_{pump,MED}$ (W)	273.7	213.3	103.6
Net power density, $P_{d,net}$ (W/m$^2_{cp}$)	1.9	2.2	4.3
Waste heat rate, $\dot{Q}_{wh}$ (kW)	37	34.9	17.9
MED STEC, sE (kWh/m^3)	35.6	31.7	35.4

The exergy balance of the most-performing case (obtained when using high-performing membranes), is depicted in Fig. 12 by means of a Grassmann diagram. For each component of the system, entering and exiting exergy rate flows are presented, together with the amount of exergy destroyed. In the RED unit, the exergy rate content of the concentrate and dilute solutions (2493 W) is partly consumed to generate electric power (1080 W), with the remaining fraction destroyed due to the irreversibility sources of the pile (887 W, 28.5% of the total exergy destruction). Then, a fraction of the electric power produced is used to drive the RED and MED pumps (2 W and 104 W, respectively).

The exergy rate content of the solution exiting the RED unit (528 W) is then marginally destroyed within Mixer 1 (0.1 W, value practically negligible compared to the exergy destruction within the RED and MED units). In the MED unit, the exergy rate supplied by the cooling process (489 W) is added to the waste heat exergy rate (3597 W) and pumping exergy rate (104 W), destroying a large amount of exergy (2191 W, 70.4% of the total). A large amount of waste heat exergy is supplied to the system compared to the net electric power produced in the RED unit, leading to a low value of the thermal efficiency (5.4%). In contrast to the case where reference membranes are used, here the MED unit limits the overall exergy efficiency of the system. The exergy rate of Mixer 1 outlet solution is significantly increased in the MED unit (from 526 W to 2525 W). Finally, the exergy rate of the distillate is partially diminished in Mixer 2 (from 434 W to 402 W), where the salinity of the dilute solution is restored and a small amount of the exergy rate is destroyed (34 W).

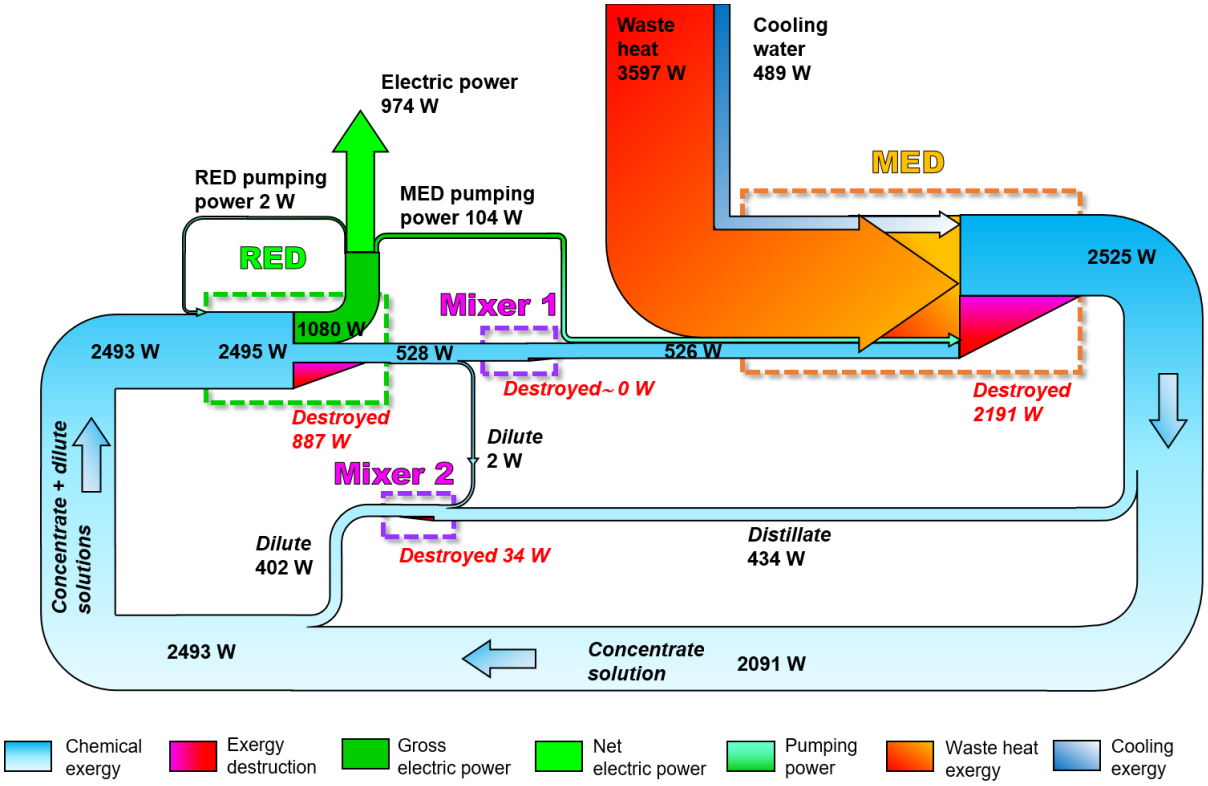

Fig. 12. Grassmann diagram of the RED-MED system, showing the values of exergy flows calculated using high-performing membranes and the best-performing operating conditions analysed.

4. CONCLUSIONS

In this work, for the first time, a detailed exergy analysis of a RED-MED HE has been carried out. Comprehensive mathematical models of the RED and MED units were used, which allowed performing sensitivity analyses on the main operating and design variables of the system: inlet solutions concentration, velocity, and membrane's aspect ratio.

The inlet solutions concentration and velocity in the RED unit, together with the aspect ratio of the membranes, have an important influence on the performance of the RED-MED HE. The overall exergy efficiency could be almost doubled by selecting the most-performing values of the operating and design parameters (C_{HC}=4 M, C_{LC}=0.01 M, v_{HC}=0.2 cm/s, v_{LC}=0.5 cm/s, b=0.5 m, L=0.5 m, and 26 MED effects) among those investigated in the parametric analysis.

The results of the exergy analysis indicate that the component with major contribution to the overall exergy destruction is the MED unit (about 70% of total), followed by the RED unit (25 – 30%) and to a lesser extent, Mixer 1 and Mixer 2. Moreover, exergy destruction in the RED

unit related to the permselectivity of the membranes, salt diffusive flux and water osmotic flux were found to greatly decrease the overall RED-MED HE performance. On the contrary, the effect of polarization phenomena and RED pumping power consumption only produce a slight reduction in efficiency. The influence of the MED pumping power is more accused than the latter, leading to an important decrease in the global exergy efficiency. In order to reduce the irreversibilities associated with the structural parameters in the RED unit, further research on the improvement of the membrane properties should be taken into consideration. The irreversibilities associated with the MED unit have been related to the temperature differences in the heat exchangers, which has to be kept as low as possible to minimise exergy losses, although higher specific heat transfer areas and higher capital cost investments are expected in that case.

Finally, the energy conversion potential of the technology was assessed using high-performing membranes, reaching a global exergy efficiency of 23.8% (5.4% thermal), showing the significant potential of the RED-MED HE for the conversion of waste heat into electricity. Future work will extend the model including also an economic and environmental analysis in order to demonstrate the techno-economic and environmental feasibility of the process.

Acknowledgments

This work has been performed within the RED-Heat-to-Power project (Conversion of Low Grade Heat to Power through closed loop Reverse Electro-Dialysis) – Horizon 2020 program, Grant Agreement no. 640667.

The authors would like to acknowledge also FujiFilm Manufacturing Europe B.V. for their support and for providing information on ion exchange membranes properties.

NOMENCLATURE

Variables

A	Area, m^2
a	Activity, -
b	Membrane's width, m
C	Molar concentration, mol/L
c	Specific heat capacity, J/(kg·°C)
E	Electric voltage, V
$\bar{e}$	Molar flow exergy, J/mol
$\dot{E}$	Exergy rate, W

F	Faraday constant, C/mol
h	Specific enthalpy, J/kg
$\bar{h}$	Molar enthalpy, J/mol
i, I	Electric current, A
J	Molar flux, mol/(m^2·s)
L	Length, m
M	Molar mass, g/mol
m	Molality, mol/kg
$\dot{m}$	Mass flow rate, kg/s
$\dot{N}$	Molar flow rate, mol/s
n_h	Hydration number, -
p	Pressure, Pa
P	Power, W
P_s	Salt permeability coefficient, m^2/s
P_w	Water permeability, m/(Pa·s)
Q	Volumetric flow rate, m^3/s
R	Areal electrical resistance, Ω·m^2
	or gas constant, J/(mol·K)
R_L	External resistance (load), Ω
sA	Specific heat transfer area, m^2/(kg/s)
sE	Specific thermal energy, kWh/m$^3_{dist}$
$\bar{s}$	Molar entropy, J/(mol·K)
s_f	Spacer shadow factor, -
T, t	Temperature, °C (or K)
U	Overall heat transfer coefficient, W/(m^2·K)
v	Velocity of the solutions, cm/s
X	Salinity, ppm
x	Molar fraction (-) or distance (m)

Acronyms and abbreviations

AEM	Anion Exchange Membrane
BPE	Boiling Point Elevation
CEM	Cation Exchange Membrane
EES	Engineering Equation Solver
HC	High Concentration
HE	Heat Engine
IEM	Ion Exchange Membrane
LC	Low Concentration
MD	Membrane Distillation
MED	Multi-Effect Distillation
OCV	Open Circuit Voltage

ORC	Organic Rankine Cycle
RDS	Restricted Dead State
RED	Reverse Electrodialysis
SGE	Salinity Gradient Engine

Greek

α	Permselectivity, -, or mass fraction, -
γ	Activity coefficient, -
δ	Thickness, m
ϵ	Relative volume, -, or tolerance, -
η	Efficiency, %
θ	Polarization coefficient, -
Λ	Equivalent conductivity, $S \cdot cm^2/mol$
λ	Enthalpy of vaporization, J/kg
μ	Chemical potential, J/mol
ν	Number of ions
ρ	Density, kg/m^3
ϕ	Osmotic coefficient, -

Subscripts

0	Dead state
av	Average
B	Brine
c	Condensate
ch	Chemical
coul	Coulombic
cp	Cell pair
cw	Cooling water
d	Density
D	Destroyed
diff	Diffusive
dist	Distillate
eosm	Electro-osmotic
F	Feedwater or Fuel
FB	Flash in flashing box
FE	Flash in the effect
g	Global
H	Height
HC	High concentration
in	Inlet or internal
L	Loss or Load

LC	Low concentration
M	Mixer
m	Membrane
net	Net value
osm	Osmotic
P	Product or Power
p	Pumping or pressure
ph	Physical
preh	Preheater
pump	Related to pumping
Q	heat
s	Salt
sat	Saturated
T	Total
th	Thermal
V	Vapor
w	Water
wh	Waste heat
X	Related to exergy

Superscripts

′	Conditions after the demister
″	Conditions in the flash box
0	Dead state
*	Restricted dead state

REFERENCES

[1] Kermani M, Wallerand AS, Kantor ID, Maréchal F. Generic superstructure synthesis of organic Rankine cycles for waste heat recovery in industrial processes. Appl Energy 2018;212:1203–25. doi:10.1016/j.apenergy.2017.12.094.

[2] Wick GL. Power from salinity gradients. Energy 1978;3:95–100. doi:10.1016/0360-5442(78)90059-2.

[3] Post JW, Veerman J, Hamelers HVM, Euverink GJW, Metz SJ, Nymeijer K, et al. Salinity-gradient power: Evaluation of pressure-retarded osmosis and reverse electrodialysis. J Memb Sci 2007;288:218–30. doi:10.1016/j.memsci.2006.11.018.

[4] Maigrot E, Sabates J. Apparat zur Läuterung von Zuckersäften mittels Elektrizität. German Patent nº 50443, 1890.

[5] Pattle RE. Production of Electric Power by mixing Fresh and Salt Water in the Hydroelectric Pile. Nature 1954;174:660–660. doi:10.1038/174660a0.

[6] Weinstein JN, Leitz FB. Electric Power from Differences in Salinity: The Dialytic Battery. Science (80-) 1976;191:557–9. doi:10.1126/science.191.4227.557.

[7] Jagur-Grodzinski J, Kramer R. Novel process for direct conversion of free energy of mixing into electric power. Ind Eng Chem Process Des Dev 1986;25:443–9. doi:10.1021/i200033a016.

[8] Veerman J, Post JW, Saakes M, Metz SJ, Harmsen GJ. Reducing power losses caused by ionic shortcut currents in reverse electrodialysis stacks by a validated model. J Memb Sci 2008;310:418–30. doi:10.1016/j.memsci.2007.11.032.

[9] Vermaas DA, Saakes M, Nijmeijer K. Doubled Power Density from Salinity Gradients at Reduced Intermembrane Distance. Environ Sci Technol 2011;45:7089–95. doi:10.1021/es2012758.

[10] Daniilidis A, Vermaas DA, Herber R, Nijmeijer K. Experimentally obtainable energy from mixing river water, seawater or brines with reverse electrodialysis. Renew Energy 2014;64:123–31. doi:10.1016/J.RENENE.2013.11.001.

[11] Long R, Li B, Liu Z, Liu W. Performance analysis of reverse electrodialysis stacks: Channel geometry and flow rate optimization. Energy 2018;158:427–36. doi:10.1016/J.ENERGY.2018.06.067.

[12] Long R, Li B, Liu Z, Liu W. Reverse electrodialysis: Modelling and performance analysis based on multi-objective optimization. Energy 2018;151:1–10. doi:10.1016/J.ENERGY.2018.03.003.

[13] Tedesco M, Scalici C, Vaccari D, Cipollina A, Tamburini A, Micale G. Performance of the first reverse electrodialysis pilot plant for power production from saline waters and concentrated brines. J Memb Sci 2016;500:33–45. doi:10.1016/j.memsci.2015.10.057.

[14] Loeb S. Method and apparatus for generating power utilizing reverse electrodialysis. US4171409A, 1979.

[15] Conversion of Low Grade Heat to Power through closed loop Reverse ElectroDialysis—Horizon 2020 programme, Project Number: 640667: www.red-heat-to-power.eu n.d. https://cordis.europa.eu/project/rcn/193740_en.html (accessed September 4, 2018).

[16] El-Sayed YM, Silver RS. Chapter 2 – Fundamentals of Distillation. In: Spiegler KS, Laird ADK, editors. Princ. Desalin., Academic Press; 1980, p. 55–109. doi:10.1016/B978-0-12-656701-4.50008-5.

[17] El-Dessouky H, Alatiqi I, Bingulac S, Ettouney H. Steady-state analysis of the multiple effect evaporation desalination process. Chem Eng Technol 1998;21:437–51. doi:10.1002/(SICI)1521-4125(199805)21:5<437::AID-CEAT437>3.0.CO;2-D.

[18] Mistry KH, Antar MA, Lienhard JH. An improved model for multiple effect distillation. Desalin Water Treat 2013;51:807–21. doi:10.1080/19443994.2012.703383.

[19] Ortega-Delgado B, García-Rodríguez L, Alarcón-Padilla D-C. Opportunities of improvement of the MED seawater desalination process by pretreatments allowing high-temperature operation. Desalin Water Treat 2017;97. doi:10.5004/dwt.2017.21679.

[20] Luo X, Cao X, Mo Y, Xiao K, Zhang X, Liang P, et al. Power generation by coupling reverse electrodialysis and ammonium bicarbonate : Implication for recovery of waste heat. Electrochem Commun 2012;19:25–8. doi:10.1016/j.elecom.2012.03.004.

[21] Cusick RD, Kim Y, Logan BE. Energy capture from thermolytic solutions in microbial reverse-electrodialysis cells. Science 2012;335:1474–7. doi:10.1126/science.1219330.

[22] Kwon K, Park BH, Kim DH, Kim D. Parametric study of reverse electrodialysis using ammonium bicarbonate solution for low-grade waste heat recovery. Energy Convers Manag 2015;103:104–10. doi:10.1016/J.ENCONMAN.2015.06.051.

[23] Hatzell MC, Ivanov I, D. Cusick R, Zhu X, Logan BE. Comparison of hydrogen production and electrical power generation for energy capture in closed-loop ammonium bicarbonate reverse electrodialysis systems. Phys Chem Chem Phys 2014;16:1632–8. doi:10.1039/c3cp54351j.

[24] Bevacqua M, Carubia A, Cipollina A, Tamburini A, Tedesco M, Micale G. Performance of a RED system with ammonium hydrogen carbonate solutions. Desalin Water Treat 2016;57:23007–18. doi:10.1080/19443994.2015.1126410.

[25] Bevacqua M, Tamburini A, Papapetrou M, Cipollina A, Micale G, Piacentino A. Reverse electrodialysis with NH4HCO3-water systems for heat-to-power conversion. Energy 2017;137:1293–307. doi:10.1016/J.ENERGY.2017.07.012.

[26] Long R, Li B, Liu Z, Liu W. Hybrid membrane distillation-reverse electrodialysis electricity generation system to harvest low-grade thermal energy. J Memb Sci 2017;525:107–15. doi:10.1016/j.memsci.2016.10.035.

[27] Micari M, Cipollina A, Giacalone F, Kosmadakis G, Papapetrou M, Zaragoza G, et al. Towards the first proof of the concept of a Reverse ElectroDialysis - Membrane Distillation Heat Engine. Desalination 2019;453:77–88. doi:10.1016/j.desal.2018.11.022.

[28] Tamburini A, Tedesco M, Cipollina A, Micale G, Ciofalo M, Papapetrou M, et al. Reverse electrodialysis heat engine for sustainable power production. Appl Energy 2017;206:1334–53. doi:10.1016/J.APENERGY.2017.10.008.

[29] Giacalone F, Catrini P, Tamburini A, Cipollina A, Piacentino A, Micale G. Exergy analysis of reverse electrodialysis. Energy Convers Manag 2018;164:588–602. doi:10.1016/j.enconman.2018.03.014.

[30] Hu J, Xu S, Wu X, Wu D, Jin D, Wang P, et al. Theoretical simulation and evaluation for the performance of the hybrid multi-effect distillation—reverse electrodialysis power generation system. Desalination 2018;443:172–83. doi:10.1016/j.desal.2018.06.001.

[31] Palenzuela P, Micari M, Ortega-Delgado B, Giacalone F, Zaragoza G, Alarcón-Padilla D-C, et al. Performance Analysis of a RED-MED Salinity Gradient Heat Engine. Energies 2018;11:3385. doi:10.3390/en11123385.

[32] Giacalone F, Olkis C, Santori G, Cipollina A, Brandani S, Micale G. Novel solutions for closed-loop reverse electrodialysis: Thermodynamic characterisation and perspective analysis. Energy 2019;166:674–89. doi:10.1016/j.energy.2018.10.049.

[33] Bi Y, Wang X, Liu Y, Zhang H, Chen L. Comprehensive exergy analysis of a ground-source heat pump system for both building heating and cooling modes. Appl Energy 2009;86:2560–5. doi:10.1016/j.apenergy.2009.04.005.

[34] Erbay Z, Hepbasli A. Application of conventional and advanced exergy analyses to evaluate the performance of a ground-source heat pump (GSHP) dryer used in food drying. Energy Convers Manag 2014;78:499–507. doi:10.1016/j.enconman.2013.11.009.

[35] Dai Y, Wang J, Gao L. Parametric optimization and comparative study of organic Rankine cycle (ORC) for low grade waste heat recovery. Energy Convers Manag

2009;50:576–82. doi:10.1016/J.ENCONMAN.2008.10.018.

[36] Karellas S, Braimakis K. Energy-exergy analysis and economic investigation of a cogeneration and trigeneration ORC-VCC hybrid system utilizing biomass fuel and solar power. Energy Convers Manag 2016;107:103–13. doi:10.1016/j.enconman.2015.06.080.

[37] Wang J, Dai Y, Gao L. Exergy analyses and parametric optimizations for different cogeneration power plants in cement industry. Appl Energy 2009;86:941–8. doi:10.1016/j.apenergy.2008.09.001.

[38] Ahmadi P, Dincer I, Rosen MA. Exergy, exergoeconomic and environmental analyses and evolutionary algorithm based multi-objective optimization of combined cycle power plants. Energy 2011;36:5886–98. doi:10.1016/j.energy.2011.08.034.

[39] Ogorure OJ, Oko COC, Diemuodeke EO, Owebor K. Energy, exergy, environmental and economic analysis of an agricultural waste-to-energy integrated multigeneration thermal power plant. Energy Convers Manag 2018;171:222–40. doi:10.1016/j.enconman.2018.05.093.

[40] Hepbasli A. Low exergy (LowEx) heating and cooling systems for sustainable buildings and societies. Renew Sustain Energy Rev 2012;16:73–104. doi:10.1016/j.rser.2011.07.138.

[41] Zhou Y. Evaluation of renewable energy utilization efficiency in buildings with exergy analysis. Appl Therm Eng 2018;137:430–9. doi:10.1016/j.applthermaleng.2018.03.064.

[42] Torío H, Angelotti A, Schmidt D. Exergy analysis of renewable energy-based climatisation systems for buildings: A critical view. Energy Build 2009;41:248–71. doi:10.1016/j.enbuild.2008.10.006.

[43] Emdadi A, Zenouzi M, Kowalski GJ. Determining the Potential of Salinity Gradient Energy Source Using an Exergy Analysis 2016:V001T07A003.

[44] Hepbasli A. A key review on exergetic analysis and assessment of renewable energy resources for a sustainable future. Renew Sustain Energy Rev 2008;12:593–661. doi:10.1016/J.RSER.2006.10.001.

[45] Klein SA. Engineering Equation Solver Software (EES) 2013.

[46] Cerva M La, Liberto M Di, Gurreri L, Tamburini A, Cipollina A, Micale G, et al. Coupling CFD with a one-dimensional model to predict the performance of reverse electrodialysis stacks. J Memb Sci 2017;541:595–610. doi:10.1016/j.memsci.2017.07.030.

[47] Tedesco M, Cipollina A, Tamburini A, Bogle IDL, Micale G. A simulation tool for

analysis and design of reverse electrodialysis using concentrated brines. Chem Eng Res Des 2015;93:441–56. doi:10.1016/j.cherd.2014.05.009.

[48] El-Dessouky HT, Ettouney HM. Fundamentals of Salt Water Desalination. Elsevier; 2002.

[49] Pitzer KS, Peiper JC, Busey RH. Thermodynamic Properties of Aqueous Sodium Chloride Solutions. J Phys Chem Ref Data 1984. doi:10.1063/1.555709.

[50] Fitzsimons L, Corcoran B, Young P, Foley G. Exergy analysis of water purification and desalination: A study of exergy model approaches. Desalination 2015;359:212–24. doi:10.1016/j.desal.2014.12.033.

[51] Bejan A, Tsatsaronis G, Moran MJ. Thermal Design and Optimization. New York Etc.: John Wiley and Sons; 1996.

[52] Pitzer KS. Activity Coefficients in Electrolyte Solutions. Boca Raton: CRC Press; 1991. doi:10.1201/9781351069472.

[53] Piacentino A. Application of advanced thermodynamics, thermoeconomics and exergy costing to a Multiple Effect Distillation plant: In-depth analysis of cost formation process. Desalination 2015;371:88–103. doi:10.1016/j.desal.2015.06.008.

[54] Tsatsaronis G. Thermoeconomic analysis and optimization of energy systems. Prog Energy Combust Sci 1993;19:227–57. doi:10.1016/0360-1285(93)90016-8.

[55] Kotas TJ. The exergy method of thermal plant analysis. Butterworths; 1985.

[56] Torres C, Valero A, Rangel V, Zaleta A. On the cost formation process of the residues. Energy 2008;33:144–52. doi:10.1016/J.ENERGY.2007.06.007.

[57] Piacentino A. Application of advanced thermodynamics, thermoeconomics and exergy costing to a Multiple Effect Distillation plant: In-depth analysis of cost formation process. Desalination 2015;371:88–103. doi:10.1016/j.desal.2015.06.008.

[58] Shahzad MW, Burhan M, Ang L, Ng KC. Energy-water-environment nexus underpinning future desalination sustainability. Desalination 2017;413:52–64. doi:10.1016/J.DESAL.2017.03.009.

[59] Rogers PSZ, Pitzer KS. Volumetric Properties of Aqueous Sodium Chloride Solutions. J Phys Chem Ref Data 1982;11:15–81. doi:10.1063/1.555660.

[60] Vitagliano V, Lyons PA. Diffusion Coefficients for Aqueous Solutions of Sodium Chloride and Barium Chloride. J Am Chem Soc 1956. doi:10.1021/ja01589a011.

[61] Ozbek H. Viscosity of aqueous sodium chloride solutions from 0 – 150°C. Am. Chem. Soc. 29th Southeast Reg. Meet., 1971. doi:LBNL Paper LBNL-3553E.

[62] Gurreri L, Tamburini A, Cipollina A, Micale G, Ciofalo M. Flow and mass transfer in

spacer-filled channels for reverse electrodialysis: a CFD parametrical study. J Memb Sci 2016;497:300–17. doi:10.1016/j.memsci.2015.09.006.

[63] Tufa RA, Pawlowski S, Veerman J, Bouzek K, Fontananova E, di Profio G, et al. Progress and prospects in reverse electrodialysis for salinity gradient energy conversion and storage. Appl Energy 2018;225:290–331. doi:10.1016/J.APENERGY.2018.04.111.

[64] Gurreri L, Tamburini A, Cipollina A, Micale G, Ciofalo M. CFD prediction of concentration polarization phenomena in spacer-filled channels for reverse electrodialysis. J Memb Sci 2014;468:133–48. doi:10.1016/j.memsci.2014.05.058.

[65] Kakaç S, Liu H, Pramuanjaroenkij A. Heat Exchangers: Selection, Rating, and Thermal Design. Boca Raton, FL: CRC Press; 2002. doi:10.1016/0378-3820(89)90046-5.

Appendix A

A.1 Osmotic and activity coefficients

The model from Pitzer et al. [49] has been selected for the calculation of the mean activity coefficient γ (-) and the osmotic coefficient ϕ (-) of the NaCl aqueous solution, determined by Eqs. (A.1) and (A.2), respectively:

$$ln\gamma = -|z_M z_X| A_\phi \left(\frac{I^{0.5}}{1 + bI^{0.5}} + \frac{2}{b} \ln(1 + bI^{0.5}) \right) + 2m \frac{\nu_M \nu_X}{\nu} \cdot \cdot \left\{ 2\beta_{MX}^{(0)} + \frac{2\beta_{MX}^{(1)}}{\alpha^2 I} \left[1 - \left(1 + \alpha I^{0.5} - \frac{\alpha^2 I}{2} \right) \cdot \exp(-\alpha I^{0.5}) \right] \right\} + 3m^2 \frac{(\nu_M \nu_X)^{3/2}}{\nu} C_{MX}^{\phi} \quad \text{(A.1)}$$

$$\phi - 1 = -|z_M z_X| A_\phi \frac{I^{0.5}}{1 + bI^{0.5}} + m \frac{2\nu_M \nu_X}{\nu} \left[\beta_{MX}^{(0)} + \beta_{MX}^{(1)} \exp(-\alpha I^{0.5}) \right] + 2m^2 \frac{(\nu_M \nu_X)^{3/2}}{\nu} C_{MX}^{\phi} \quad \text{(A.2)}$$

where z_M and z_X are the charge of the cation and anion, respectively, A_ϕ (kg/mol)$^{0.5}$ is the Debye-Hückel parameter for the osmotic coefficient, I (mol/kg) is the ionic strengh, m (mol/kg) is the molality, ν_M and ν_X are the number of cations and anions of the salt, ν is the number of ions, $\beta_{MX}^{(0)}$, $\beta_{MX}^{(1)}$, and C_{MX}^{ϕ} are adjustable parameters (with values of 0.07525, 0.2769 and 0.0014, respectively), α is a constant (2 for univalent ions), and b is a universal parameter (1.2 kg$^{1/2}$mol$^{-1/2}$).

A.2 Thermodynamic properties of NaCl-water solution

Density

The density ρ (kg/m^3) of the aqueous NaCl solution has been determined using Eq. (A.3), obtained from the work of Rogers & Pitzer [59], as a function of the molarity C (mol/m^3) and temperature T (°C) of the solution.

$$\rho = A + B \tag{A.3}$$

$$A = 1.003 \cdot 10^{3} - 1.373 \cdot 10^{-2} \cdot T - 6.671 \cdot 10^{-3} \cdot T^{2} + 3.840 \cdot 10^{-5} \cdot T^{3} - 1.616 \cdot 10^{-7} \cdot T^{4} \tag{A.4}$$

$$B = 3.905 \cdot 10^{1} \cdot C - 7.903 \cdot 10^{-2} \cdot C \cdot T + 1.171 \cdot 10^{-3} \cdot C \cdot T^{2} - 8.444 \cdot 10^{-7} \cdot C \cdot T^{3} - 9.374 \cdot 10^{-5} \cdot C^{2} \cdot T^{2} \tag{A.5}$$

Conductivity

In order to determine the equivalent conductivity Λ_{sol} (S·cm^2·mol^{-1}) of the solutions, Eq. (A.6) has been used, dependent on the molar concentration [29]:

$$\Lambda_{sol} = \Lambda_0 - \frac{A_\Lambda \sqrt{C_{sol}}}{1 + B_\Lambda \sqrt{C_{sol}}} - C_\Lambda C_{sol} \tag{A.6}$$

where Λ_0 is the equivalent conductivity of the salt (infinite dilution), and A_Λ, B_Λ and C_Λ are specific parameters obtained for a temperature of 25 °C.

Diffusivity

The diffusion coefficient or diffusivity D (m^2/s) for NaCl aqueous solution is obtained using Eq. (A.8), obtained from [60] as a function of the solution concentration:

$$D_{sol} = 1.47 \cdot 10^{-9} + 0.13 \cdot 10^{-9} \cdot e^{-C_{sol}/70} \quad (C_{sol} \leq 400) \tag{A.7}$$

$$D_{sol} = -2.87262 \cdot 10^{-21} C_{sol}^{3} + 2.03219 \cdot 10^{-17} C_{sol}^{2} - 8.44113 \cdot 10^{-15} C_{sol} + 1.4705 \cdot 10^{-9} \quad (C_{sol} > 400) \tag{A.8}$$

Viscosity

The viscosity μ (mPa·s) of the NaCl aqueous solution has been determined by means of the correlation (A.9) proposed by Ozbek et al. [61], dependent on the temperature T (°C) and molality m (mol/kg) of the solution (valid for temperatures up to 150 °C and concentrations up to saturation).

$$\mu_{sol} = c_1 + c_2 \cdot e^{a_1 T} + c_3 \cdot e^{a_2 m} + c_4 \cdot e^{a_3 (0.01T + m)} + c_5 \cdot e^{a_4 (0.01T - m)} \tag{A.9}$$

$c_1 = 0.1256735; c_2 = 1.265347;\ c_3 = -1.105369;\ c_4 = 0.2044679;$
$c_5 = 1.308779; a_1 = -0.04296718;\ a_2 = 0.3710073;\ a_3 = 0.4230889;$
$a_4 = -0.3259828;$

A.3 Membrane properties

Electrical resistance

The areal electrical resistance R ($\Omega \cdot cm^2$) of the IEMs has been determined using quadratic empirical correlations (Eqs. (A.10) and (A.11)) obtained for FujiFilm Type 10 membranes [27], as a function of the molar concentration of the solutions:

$$R_{AEM} = 0.487\ C_{HC}^2 - 2.81\ C_{HC} + 7.21 - 0.14\ C_{LC} \quad \text{(A.10)}$$

$$R_{CEM} = 0.487\ C_{HC}^2 - 2.81\ C_{HC} + 7.22 - 0.27\ C_{LC} \quad \text{(A.11)}$$

Permselectivity

The membrane permselectivity α (-) was determined by means of empirical correlations ((A.12) and (A.13)) dependent on the molar concentration of the solutions, obtained for FujiFilm Type 10 membranes [27]:

$$\alpha_{AEM} = 0.987 - 0.0441\ C_{HC} - 0.183 C_{LC} \quad \text{(A.12)}$$

$$\alpha_{CEM} = 0.991 - 0.0441 C_{HC} - 0.253 C_{LC} \quad \text{(A.13)}$$

Polarisation coefficients

The polarisation coefficients θ (-) were calculated implementing suitable correlations obtained with data from CFD simulations for the case of Deukum GmbH spacers [62]. They are defined as the solution concentration ratio between the membrane interface and bulk plane, which can be approximated by the correlations (A.14) and (A.15):

$$\theta_{IEM,LC} = \frac{C_{m,LC}}{C_{b,LC}} \approx \left(1 + \left(\frac{2\ J_s\ \delta_{LC}}{Sh_{LC}\ D_{LC}\ C_{LC}}\right)\right)^{-1} \quad \text{(A.14)}$$

$$\theta_{IEM,HC} = \frac{C_{m,HC}}{C_{b,HC}} \approx 1 - \left(\frac{2\ J_s\ \delta_{HC}}{Sh_{HC}\ D_{HC}\ C_{HC}}\right) \quad \text{(A.15)}$$

where C_m (mol/m^3) and C_b (mol/ m^3) are the concentration in the membrane-solution interfaces and within the bulk plane (at the middle of the channel), respectively, δ (m) is the thickness of the spacer used in each channel (HC or LC); D (m^2/s) is the salt diffusivity value in the respective channel; Sh (-) is the Sherwood number, relevant to each solution, and calculated as a function of the Reynolds number Re (-) and the Schmidt number Sc (-) according to (A.16).

$$Sh = (-1.481 \cdot 10^{-7}\ Re^5 + 3.739 \cdot 10^{-5}\ Re^4 - 3.253 \cdot 10^{-3} Re^3 + 1.117 \cdot 10^{-1}\ Re^2 + 1.348 \cdot 10^{-1}\ Re + 6.954) \cdot \left(\frac{Sc}{Sc_{ref}}\right)^{0.5} \quad \text{(A.16)}$$

where Sc_{ref} is the Schmidt number of the reference solution (NaCl aqueous solution at 1 atm, 25 °C and 0.017 M).

High-performing IEMs properties

The electric resistance and permselectivity of the assumed standard reference and high-performing IEMs are compared to those of the commercial membranes found in the literature [63] in Fig. A.1, measured at the defined conditions (0.5 M for the resistance and 0.5 – 0.05 M for the permselectivity).

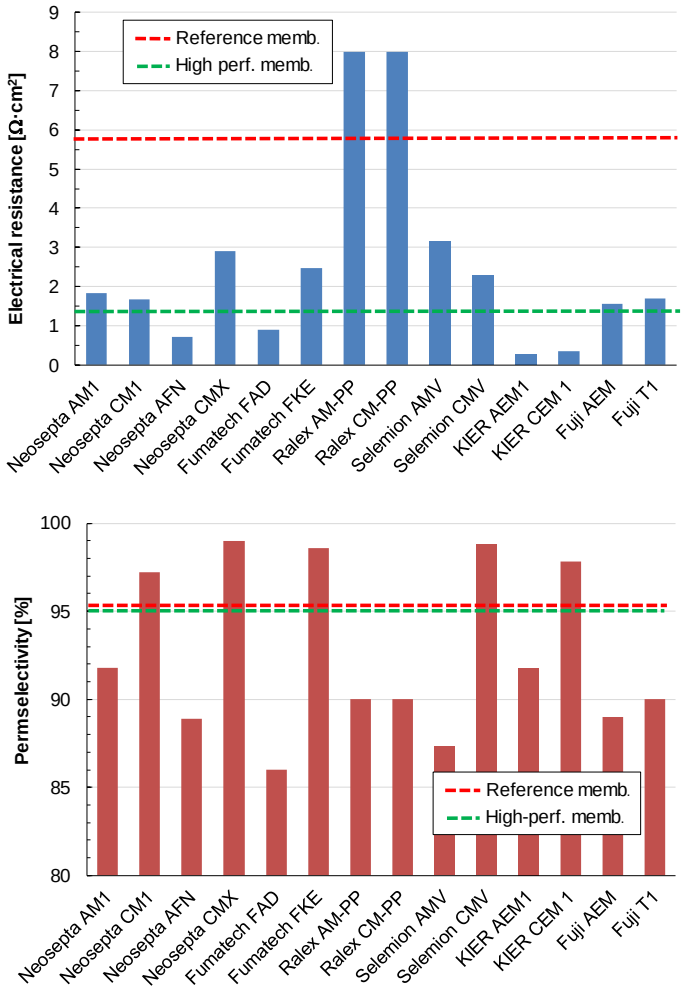

Fig. A.1 Electric membrane resistance (up) and permselectivity (down) for various commercial IEMs, measured at 0.5 M for the resistance and 0.5 – 0.05 M for the permselectivity [63]. The values for the reference and high-performing membranes properties are also represented, the latter defined as ¼ of the value measured at 0.5 M for the resistance (Eqs. (A.10) and (A.11)) and 95% for the permselectivity. It is worth noting that the permselectivity of high-performing membranes is lower than current ones at 0.5 – 0.05 M, but

it stays constant at higher concentration, while in current membranes permselectivity significantly decreases with HC concentration.

Appendix B

B.1 Pressure drop in the RED stack

The pressure drop Δp (Pa) of the solutions within the RED concentrate and dilute channels have been calculated using Eq. (B.1):

$$f = \frac{\Delta p}{L} \cdot \frac{d_h}{\frac{1}{2}\rho v^2} \tag{B.1}$$

where d_h (m) is the hydraulic diameter (=$2\delta_{channel}$), L (m) the length of the channel, ρ (kg/m^3) the density of the solution, v (m/s) the velocity of the solution, and f (-) the Fanning friction factor, calculated as a function of the Reynolds number [64].

B.2 Pumping requirements in the MED unit

For the determination of the pumping requirements within the MED, three factors have been considered, namely, the total height to be overcome ($\Delta p_{MED,H}$), the restoration of the atmospheric pressure at the exit of the HC and distillate solutions ($\Delta p_{MED,HC,out}$ and $\Delta p_{MED,dist,out}$), and the pressure drop in the cooling process ($\Delta p_{MED,cooling}$) [65]. They have been calculated by means of Eqs. (B.2), (B.3) and (B.4):

$$\Delta p_{MED,H} = \rho \cdot g \cdot H \cdot N_{eff} \tag{B.2}$$

$$\Delta p_{MED,HC,out} = \Delta p_{MED,dist,out} = p_{atm} - p_N \tag{B.3}$$

$$\Delta p_{MED,cooling} = \left(4 \cdot j_f \cdot \left(\frac{L}{d_i}\right) \cdot N_p + 4 \cdot N_p\right) \cdot \frac{1}{2}\rho v^2 \tag{B.4}$$

where H (m) is assumed to be 1 m per effect, N_{eff} (-) is the number of effects, p_N (Pa) is the pressure in the last effect, j_f (-) is the friction factor of the tube side, d_i (m) is the internal diameter of the tubes, and N_p (-) is the number of tube passes of the shell & tube condenser.